Inorg. Chem. **2007**, *46*, 8146–8161

Computational Studies of EPR Parameters for Paramagnetic Molybdenum Complexes. II. Larger Mo^V Systems Relevant to Molybdenum Enzymes

Jörg Fritscher,*,† Peter Hrobárik,‡ and Martin Kaupp*,§

Institute of Physical and Theoretical Chemistry and Center for Biological Magnetic Resonance, J. W. Goethe University of Frankfurt, Max-von-Laue-Str. 7, D-60438 Frankfurt, Germany, Institute of Inorganic Chemistry, Slovak Academy of Sciences, Dúbravská cesta 9, SK-84536 Bratislava, Slovakia, and Institut für Anorganische Chemie, Universität Würzburg, Am Hubland, D-97074 Würzburg, Germany

Received February 22, 2007

The careful validation of modern density functional methods for the computation of electron paramagnetic resonance (EPR) parameters in molybdenum complexes has been extended to a number of low-symmetry Mo^V systems that model molybdoenzyme active sites. Both *g* and hyperfine tensors tend to be reproduced best by hybrid density functionals with about 30–40% exact-exchange admixture, with no particular spin contamination problems encountered. Spin–orbit corrections to hyperfine tensors are mandatory for quantitative and, in some cases, even for qualitative agreement. The g_{11} ($g_{\|}$) component of the *g* tensor tends to come out too positive when spin–orbit coupling is included only to leading order in perturbation theory. Compared to single-crystal experiments, the calculations reproduce both *g*- and hyperfine-tensor orientations well, both relative to each other and to the molecular framework. This is significant, as simulations of the EPR spectra of natural-abundance frozen-solution samples frequently do not allow a reliable determination of the hyperfine tensors. These may now be extracted based on the quantum-chemically calculated parameters. In a number of cases, revised simulations of the experimental spectra have brought theory and experiment into substantially improved agreement. Systems with two terminal oxo ligands, and to some extent with an oxo and a sulfido ligand, have been confirmed to exhibit particularly large negative Δg_{33} shifts and thus large *g* anisotropies. This is dicussed in the context of the experimental data for xanthine oxidase.

1. Introduction

A number of molybdenum-containing enzymes, e.g., sulfite oxidase, nitrate reductase, xanthine oxidase, xanthine dehydrogenase, dimethylsulfoxide (DMSO) reductase, or polysulfide reductase, play important roles in biological two-electron redox processes.[1−4] Since these catalytic reactions directly involve the molybdenum ion, it is of great importance for a deeper understanding of the reaction mechanism to study the structure of the catalytically active molybdenum binding site.[4] The mononuclear molybdoenzymes have been subdivided into three different classes based on sequence similarities and function.[1−4] In enzymes of the sulfite oxidase class, the molybdenum ion in its fully oxidized Mo^{VI} form is coordinated by two thiolate sulfur atoms from a pyranopterindithiolate (molybdopterin), one thiolate sulfur atom from a cysteine residue, and two terminal oxo ligands. In the xanthine oxidase family, the Mo^{VI} state is coordinated to two thiolate sulfur atoms of a molybdopterin, an additional terminal sulfido ligand, a terminal oxo ligand, and one additional oxygen-containing ligand (OH_x or OR). Finally, for members of the DMSO reductase family, the coordination sphere of the Mo^{VI} form consists of four thiolate sulfur atoms from two molybdopterin cofactors, a terminal oxo or sulfido

* To whom correspondence should be addressed. E-mail: j.fritscher@epr.uni-frankfurt.de (J.F.), kaupp@mail.uni-wuerzburg.de (M.K.).
† J. W. Goethe University of Frankfurt.
‡ Slovak Academy of Sciences.
§ Universität Würzburg.

(1) Hille, R. *Chem. Rev.* **1996**, *96*, 2757.
(2) Hille, R. *Trends Biochem. Sci.* **2002**, *27*, 360.
(3) Enemark, J. H.; Cooney, J. J. A.; Wang, J.-J.; Holm, R. H. *Chem. Rev.* **2004**, *104*, 1175.
(4) *Molybdenum and Tungsten: Their Roles in Biological Processes*; Sigel, A., Sigel, H., Eds.; Marcel Dekker: New York, 2002; Vol. 39.

10.1021/ic070341e CCC: $37.00
Published on Web 08/29/2007

ligand and a serine, selenocysteine, or cysteine side chain. Due to the occurrence of paramagnetic Mo^V species during the catalytic cycles of all of these enzymes, electron paramagnetic resonance (EPR) spectroscopy[5] can be a valuable tool to reveal the structural and electronic properties of this open-shell state.[1,4,6−9] The magnetic-resonance parameters that can be extracted from EPR spectra, electronic *g* tensors, hyperfine coupling (HFC) tensors, or quadrupole coupling (QC) tensors contain indirect information about the metal binding site.[5,6,10−14] However, it is often difficult or even impossible to relate these spin Hamiltonian EPR parameters to structural information.[13,15] Furthermore, it may sometimes be hard to find a unique solution for the simulation of the EPR spectra using the spin Hamiltonian concept. Thus, models or theories are needed that are able to provide the link between molecular structure and EPR parameters. For the study of molybdoenzymes (as well as for other metalloenzymes), paramagnetic model complexes are often designed and synthesized to mimick the structure of the biological metal binding sites. Comparison of the EPR properties of these model compounds of well-known structure with EPR data from the corresponding biological systems allowed structural insight into the catalytic site of the enzyme in a number of cases.[3] The Mo^V model complexes that are the subject of this work (cf. Figure 1) have been used to investigate molybdenum binding sites in molybdoenzymes, e.g., sulfite oxidase or xanthine oxidase.[16−22] However, the development of suitable paramagnetic model systems may be very difficult or impossible in many cases. Even if potentially suitable complexes are available, the analysis and interpretation of their EPR spectra will often not be straightforward.

This is where theoretical investigations come into play. In our companion paper (in the following termed paper I),[23]

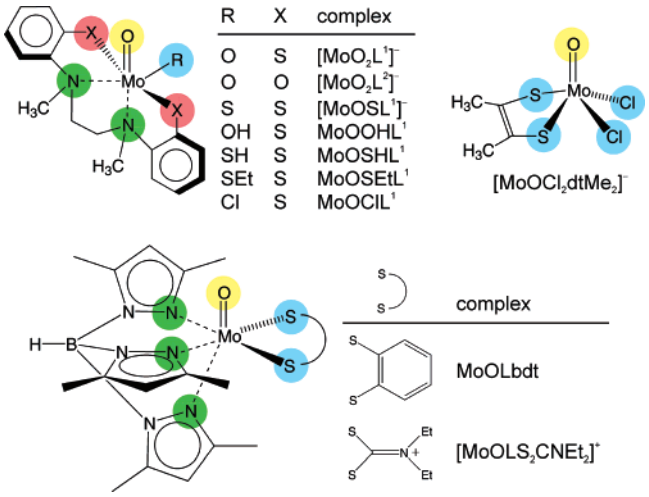

Figure 1. Schematic structures of the Mo^V model complexes studied in this work. Abbreviations: $dtMe_2$ = 1,2-dimethyl-ethene-1,2-dithiolate (dimethyldithiolene ligand), bdt = 1,2-benzenedithiolate, L^1H_2 = *N*,*N*′-bis-(2-mercaptophenyl)-*N*,*N*′-dimethyl-1,2-diaminoethane, L^2H_2 = *N*,*N*′-bis(2-hydroxyphenyl)-*N*,*N*′-dimethyl-1,2-diaminoethane, and L = tris(3,5-dimethylpyrazolyl)hydroborate.

we have pointed in detail to the growing theoretical literature on Mo^V EPR parameter interpretations, ranging from purely qualitative concepts via semiempirical relations and molecular orbital (MO) models to sophisticated quantum-chemical approaches. Quantitative computations may help to find species and structures with calculated EPR properties resembling those found experimentally, thus revealing the type and structure of the system under study. Quantum-chemical methods may also aid in the primary analysis of EPR spectra by providing precise starting parameters for spectral simulations based on spin Hamiltonians for a specific type of structure (e.g., for tensor orientations, etc.). Due to the size of the systems that have to be considered to describe the local magnetic properties of metal binding sites, density functional theory (DFT)[24] is typically the method of choice. It provides the best compromise between accuracy of the theoretical level and computation time, thus providing a very useful basis for the calculation of *g* and HFC as well as QC tensors.[23,25−35]

Until now, relatively few computational studies of *g* and molybdenum HFC tensors of Mo^V compounds have been

(5) Schweiger, A.; Jeschke, G. *Principles of Pulse Electron Paramagnetic Resonance*; Oxford University Press: Oxford, 2001.
(6) Mabbs, F. E.; Collison, D. *Electron Paramagnetic Resonance of d Transition Metal Compounds*; Elsevier Science: Amsterdam, 1992.
(7) Bray, R. C. *Q. Rev. Biophys.* **1988**, *21*, 299.
(8) Astashkin, A. V.; Feng, C.; Raitsimring, A. M.; Enemark, J. H. *J. Am. Chem. Soc.* **2005**, *127*, 502.
(9) Astashkin, A. V.; Hood, B. L.; Feng, C.; Hille, R.; Mendel, R. R.; Raitsimring, A. M.; Enemark, J. H. *Biochemistry* **2005**, *44*, 13274.
(10) Gordy, W. *Theory and Applications of Electron Spin Resonance*; John Wiley & Sons: New York, 1980.
(11) Prisner, T.; Lyubenova, S.; Atabay, Y.; MacMillan, F.; Kröger, A.; Klimmek, O. *J. Biol. Inorg. Chem.* **2003**, *8*, 419.
(12) Bennati, M.; Hertel, M. M.; Fritscher, J.; Prisner, T. F.; Weiden, N.; Hofweber, R.; Spoerner, M.; Horn, G.; Kalbitzer, H.-R. *Biochemistry* **2006**, *45*, 42.
(13) Schiemann, O.; Fritscher, J.; Kisseleva, N.; Sigurdsson, S. T.; Prisner, T. F. *ChemBioChem* **2003**, *4*, 1057.
(14) Bennati, M.; Prisner, T. F. *Rep. Prog. Phys.* **2005**, *68*, 411.
(15) Fritscher, J.; Artin, E.; Wnuk, S.; Bar, G.; Robblee, J. H.; Kacprzak, S.; Kaupp, M.; Griffin, R. G.; Bennati, M.; Stubbe, J. *J. Am. Chem. Soc.* **2005**, *127*, 7729.
(16) Peng, G.; Nichols, J.; McCullough, E. A., Jr.; Spence, J. T. *Inorg. Chem.* **1994**, *33*, 2857.
(17) Wilson, G. L.; Greenwood, R. J.; Pilbrow, J. R.; Spence, J. T.; Wedd, A. G. *J. Am. Chem. Soc.* **1991**, *113*, 6803.
(18) Mader, M. L.; Carducci, M. D.; Enemark, J. H. *Inorg. Chem.* **2000**, *39*, 525.
(19) Dhawan, I. K.; Enemark, J. H. *Inorg. Chem.* **1996**, *35*, 4873.
(20) Barnard, K. R.; Bruck, M.; Huber, S.; Grittini, C.; Enemark, J. H.; Gable, R. W.; Wedd, A. G. *Inorg. Chem.* **1997**, *36*, 637.
(21) Cosper, M. M.; Neese, F.; Astashkin, A. V.; Carducci, M. D.; Raitsimring, A. M.; Enemark, J. H. *Inorg. Chem.* **2005**, *44*, 1290.
(22) Lim, B. S.; Willer, M. W.; Miao, M.; Holm, R. H. *J. Am. Chem. Soc.* **2001**, *123*, 8343.
(23) Fritscher, J.; Hrobárik, P.; Kaupp, M. *J. Phys. Chem. B* **2007**, *111*, 4616.
(24) Parr, R. G.; Yang, W. *Density-Functional Theory of Atoms and Molecules*; Oxford University Press: New York, 1989.
(25) Kaupp, M., Malkin, V. G., Bühl, M., Eds. *Calculation of NMR and EPR Parameters*; Wiley-VCH: Weinheim, Germany, 2004.
(26) Schreckenbach, G.; Ziegler, T. *J. Phys. Chem A* **1997**, *101*, 3388.
(27) van Lenthe, E.; van der Avoird, A.; Wormer, P. E. S. *J. Chem. Phys.* **1998**, *108*, 4783.
(28) Arratia-Perez, R.; Case, D. A. *J. Chem. Phys.* **1983**, *79*, 4939.
(29) Patchkovskii, S.; Ziegler, T. *J. Am. Chem. Soc.* **2000**, *122*, 3506.
(30) Neese, F. *J. Chem. Phys.* **2003**, *118*, 3939.
(31) Neese, F. *J. Chem. Phys.* **2001**, *115*, 11080.
(32) Malkina, O. L.; Vaara, J.; Schimmelpfennig, B.; Munzarová, M.; Malkin, V. G.; Kaupp, M. *J. Am. Chem. Soc.* **2000**, *122*, 9206.
(33) Kaupp, M.; Reviakine, R.; Malkina, O. L.; Arbuznikov, A.; Schimmelpfennig, B.; Malkin, V. G. *J. Comp. Chem.* **2002**, *23*, 794.
(34) Munzarová, M. L.; Kubácek, P.; Kaupp, M. *J. Am. Chem. Soc.* **2000**, *122*, 11900.
(35) Munzarová, M.; Kaupp, M. *J. Phys. Chem. A* **1999**, *103*, 9966.

performed.[16,21,29,32,33,36−42] These works have already been discussed in paper I.[23] Only two recent theoretical studies shall be mentioned again here, since they deal with the EPR properties (*g* and molybdenum or ligand HFC or QC values) of two larger Mo^V complexes modeling the active site of molybdenum enzymes: MoOClL[1] (see Figure 1) and $[MoO(SPh)_4]^-$.[21,42] What has been lacking is a detailed quantitative calibration of modern DFT methods for an extended set of relevant low-symmetry complexes. In paper I,[23] we provided detailed validation studies on a number of small and medium-sized complexes. We were able to construct a medium-sized 12s6p5d basis set for molybdenum that is very well suited for the computation of EPR parameters and will also be used throughout this work. Furthermore, we could show that an increased amount of exact Hartree−Fock (HF) exchange in the hybrid density functional leads to an increased accuracy for *g* as well as molybdenum HFC values. Best results were generally achieved with HF exchange admixtures around 30−40%. It was found that spin−orbit (SO) corrections to the first-order isotropic and dipolar HFC constants are clearly nonnegligible and should always be taken into account to obtain accurate results. Systematic deviations of the computed "parallel" *g* shifts ($\Delta g_{||}$ or Δg_{11}) from experimental values could be attributed to higher-order relativistic effects by comparison with relativistic two-component Douglas−Kroll calculations. In addition to the principal values of the *g* and HFC tensors, their relative orientation as well as absolute orientation in the molecular frame were computed for two less-symmetrical complexes. Comparison with results from single-crystal EPR studies revealed excellent agreement. Finally, the issue of spin contamination artifacts was also discussed. In conclusion, good predictive power of the employed DFT methods was found for the investigated Mo^V species.

Here, we extend the investigations to a variety of larger low-symmetry Mo^V model complexes (Figure 1) that are relevant to molybdenum enzymes (see above).[16−22] Electronic *g* tensors and molybdenum HFC tensors for these compounds have been calculated with our recent implementations[23,33,43,44] in the *MAG-ReSpect* code,[45] using unrestricted Kohn−Sham DFT together with hybrid functionals. Comparison is made specifically with experimental data for artificial model complexes, but we also draw some conclusions relevant for binding sites in various molybdoenzymes.

2. Theoretical Formalism and Computational Details

The theoretical background of EPR spin Hamiltonian parameters and their computation is covered in detail in the literature[10,25,46−48] and is also presented in the first paper of this study.[23] Only the most relevant points will be summarized here.

***g*-Tensor Calculations.**[47] The *g* tensor **g** is calculated as the correction $\Delta\mathbf{g}$ to the free-electron *g* value g_e (in this work, $\Delta\mathbf{g}$ will be given in ppm, i.e., in units of 10^{-6})

$$\mathbf{g} = g_e\mathbf{1} + \Delta\mathbf{g}$$

with $g_e = 2.002319$. Up to the level of second-order perturbation theory within the framework of the Breit−Pauli Hamiltonian, the *g*-shift $\Delta\mathbf{g}$ consists of the terms[47,49]

$$\Delta\mathbf{g} = \Delta\mathbf{g}^{SO/OZ} + \Delta\mathbf{g}^{RMC} + \Delta\mathbf{g}^{GC}$$

of which the "paramagnetic" second-order spin−orbit/orbital Zeeman cross-term $\Delta\mathbf{g}^{SO/OZ}$ dominates (except for extremely small Δg values).[47] The relativistic mass correction term $\Delta\mathbf{g}^{RMC}$ and the one-electron part of the gauge correction term $\Delta\mathbf{g}^{GC}$ have also been included.[32,33]

Hyperfine Coupling Tensor Calculations.[47] The isotropic hyperfine coupling constant $A'_{iso}(N)$ of a nucleus *N* is at first order approximated by the Fermi contact term $A_{FC}(N) = A_{iso}(N)$. A_{iso} and the Cartesian components T_{ij} of the anisotropic dipolar tensor **T** make up the nonrelativistic first-order part of the HFC tensor

$$A_{ij}(N) = T_{ij}(N) + \delta_{ij}\cdot A_{iso}(N)$$

SO corrections to the HFC tensor arise as second-order coupling contributions, leading to a nontraceless tensor $\mathbf{A}^{SO}$. For better comparison with experimental values, the SO correction to the principal components A_{ii} of the nonrelativistic HFC tensor **A** will be given in terms of an isotropic pseudocontact (A_{PC}) and dipolar ($T_{ii,orb}$) term

$$A^{SO}_{ii}(N) = A_{PC}(N) + T_{ii,orb}(N)$$

With these definitions, the components of the complete HFC tensor **A′** (up to second-order perturbation theory) can be written as

$$A'_{ij}(N) = T_{ij}(N) + T_{ij,orb}(N) + \delta_{ij}(A_{FC}(N) + A_{PC}(N)) = T'_{ij}(N) + \delta_{ij}\cdot A'_{iso}(N)$$

The quantities A'_{iso} and T'_{ii} (including SO corrections) represent our best description of the experimental EPR parameters and should therefore be used for comparison with experimental data. In the following, we will generally refer to the molybdenum hyperfine interaction and argument *N* will be omitted. Furthermore, the T_{ii}, $T_{ii,orb}$, and T'_{ii} values will always be given as eigenvalues of the corresponding tensors, i.e., in their own principal axis systems. The sum relation $T'_{ii} = T_{ii} + T_{ii,orb}$ will only be fully valid if the principal axis systems of all three tensors coincide. Since this is not the case for less-symmetrical compounds, T'_{ii} will in general deviate from

(36) Sunil, K. K.; Harrison, J. F.; Rogers, M. T. *J. Chem. Phys.* **1982**, *76*, 3087.
(37) Swann, J.; Westmoreland, T. D. *Inorg. Chem.* **1997**, *36*, 5348.
(38) Li, W.; Hong, M.; Cao, R.; Kang, B.; Liu, H. *J. Magn. Reson.* **1999**, *138*, 80.
(39) Patchkovskii, S.; Ziegler, T. *J. Chem. Phys.* **1999**, *111*, 5730.
(40) Patchkovskii, S.; Ziegler, T. *J. Phys. Chem A* **2001**, *105*, 5490.
(41) Arbuznikov, A. V.; Kaupp, M.; Malkin, V. G.; Reviakine, R.; Malkina, O. L. *Phys. Chem. Chem. Phys.* **2002**, *4*, 5467.
(42) Astashkin, A. V.; Neese, F.; Raitsimring, A. M.; Cooney, J. J. A.; Bultman, E.; Enemark, J. H. *J. Am. Chem. Soc.* **2005**, *127*, 16713.
(43) Arbuznikov, A. V.; Vaara, J.; Kaupp, M. *J. Chem. Phys.* **2004**, *120*, 2127.
(44) Remenyi, C.; Reviakine, R.; Arbuznikov, A. V.; Vaara, J.; Kaupp, M. *J. Phys. Chem. A* **2004**, *108*, 5026.
(45) Malkin, V. G.; Malkina, O. L.; Reviakine, R.; Arbuznikov, A. V.; Kaupp, M.; Schimmelpfennig, B.; Malkin, I.; Helgaker, T.; Ruud, K., *MAG-ReSpect*, version 1.2, 2004.
(46) Abragam, A.; Bleaney, B. *Electron Paramagnetic Resonance of Transition Ions*; Oxford Clarendon Press: Oxford, U.K., 1970.
(47) Harriman, J. E. *Theoretical Foundations of Electron Spin Resonance*; Academic Press: New York, 1978.
(48) Weltner, W., *Magnetic Atoms and Molecules*; Dover Publications: New York, 1983.
(49) Moss, R. E. *Advanced Molecular Quantum Mechanics*; Chapman and Hall: London, 1973.

the sum of the two eigenvalues T_{ii} and $T_{ii,\mathrm{orb}}$. The size of this deviation is an indicator of how much the axis systems differ from each other.

Calculation of EPR Parameters. In practice, the *g*- and HFC-tensor calculations were carried out in two steps: first, the unrestricted Kohn−Sham orbitals were generated with the *Gaussian 03* program.[50] These were transferred by suitable interface routines to the in-house *MAG-ReSpect* property package,[45] which was used to carry out the *g*-tensor and HFC-tensor calculations.

In *Gaussian 03*, single-point self-consistent field (SCF) calculations, tight SCF convergence criteria (energy and density matrix convergence 10^{-6} and 10^{-8} a.u., respectively), and an ultrafine integration grid (99 radial shells and 590 angular points per shell) were used. For molybdenum, the medium-sized 12s6p5d basis set constructed and tested in paper I[23] was used. It is based on the all-electron TZVP basis set by Ahlrichs and May.[51] Huzinaga−Kutzelnigg-type IGLO-II basis sets[52] were used for all other atoms. The following exchange-correlation functionals were used and compared: (a) the local density approximation (LDA) in the form of Slater exchange and the Vosko−Wilk−Nusair correlation functional[53] (VWN, corresponding to the VWN5 keyword in *Gaussian 03*); (b) the BP86[54−56] GGA (generalized gradient approximation) functional; (c) the B3PW91[57−60] hybrid functional, incorporating 20% exact Hartree−Fock (HF) exchange; and (d) user-defined one-parameter BPW91-based hybrid functionals (as available from the *Gaussian 03* program) of the general form

$$E_{\mathrm{XC}}^{\mathrm{hybrid}} = a_0 E_{\mathrm{X}}^{\mathrm{HF}} + (1 - a_0) E_{\mathrm{X}}^{\mathrm{B88}} + E_{\mathrm{C}}^{\mathrm{PW91}}$$

with a_0 indicating the amount of Hartree−Fock exact exchange $E_{\mathrm{X}}^{\mathrm{HF}}$ (chosen as 0.30, 0.40, 0.50, 0.60, or 0.70; in the following, denoted as BPW91-30HF, BPW91-40HF, etc.).

The property calculations in *MAG-ReSpect* employed the atomic mean-field (*AMFI*) approximation[61,62] to compute the matrix elements of the spin−orbit operator. A common gauge at the molybdenum nucleus was used for the *g* tensors.

Neglect of Scalar Relativistic Effects and Higher-Order SO Contributions. Calculations in this work neglect scalar relativistic effects on HFC and *g* tensors, as well as higher-order SO effects on *g* tensors, and errors arising from these simplifications should be kept in mind. On the basis of calculations in paper I,[23] we expect scalar relativistic effects on *g* tensors to be only of minor importance, at most ca. 3000−4000 ppm. Scalar relativistic effects on the Mo hyperfine couplings will be small for the anisotropies, at most a few megahertz (the largest effects may arise from modifications of SO contributions). In contrast, the effects on A_{iso} are more substantial: For $[MoOCl_4]^-$ and $[MoOF_5]^{2-}$, our calculations indicated an enhancement of A_{FC} by about 20%.[23] Two-component calculations of *g* tensors suggested that higher-order SO contributions affect the perpendicular components only marginally but reduce g_{11} ($g_{\parallel}$) by about 10000−20000 ppm.[23]

Molecular Structures and Structure Optimizations. EPR parameter calculations were carried out for a set of Mo^V model complexes[16−22] (Figure 1) with doublet ground states, including the "octahedral" hexacoordinated $[MoORL^1]$ (R = O, S, OH, SH, SEt, Cl)[17,18,20] and $[MoO_2L^2]$[16] with the tetradentate ligands L^1H_2 = *N*,*N*′-bis(2-mercaptophenyl)-*N*,*N*′-dimethyl-1,2-diaminoethane and L^2H_2 = *N*,*N*′-bis(2-hydroxyphenyl)-*N*,*N*′-dimethyl-1,2-diaminoethane, the also octahedral hexacoordinated [MoOL(S−R−S)] (bidentate sulfur donor ligand S−R−S = 1,2-benzenedithiolate (bdt) or S_2CNEt_2)[19] with the tridentate ligand L = tris(3,5-dimethylpyrazolyl)hydroborate (frequently abbreviated as Tp*), and the "square-pyramidal" pentacoordinated $[MoOCl_2dtMe_2]$[22] with the bidentate ligand $dtMe_2$ = 1,2-dimethyl-ethene-1,2-dithiolate. The structures of the latter two groups are close to C_s symmetry, those from the first group are close to C_2 for $[MoO_2L^{1,2}]^-$, and those for the other cases or of even lower (the local symmetry around the molybdenum center may be considered as C_{2v} or C_s, respectively, for these cases). We will discuss the results (see below) in a somewhat different ordering of complexes, consistent with their specific EPR characteristics.

The molecular coordinates of all molybdenum complexes were obtained by structure optimization (starting from crystallographic data for related systems) at unrestricted DFT level (BP86[54−56] functional) with the *Turbomole*[63] code. For molybdenum, an energy-adjusted small-core effective core potential[64] was used together with a TZVP valence basis set (7s6p5d)/[5s3p3d] (default basis in *Turbomole* for atoms from Rb to Rn). TZVP all-electron basis sets[65] were employed for all other atoms. The Coulomb term was approximated by the resolution of the identity (RI) method[66,67] (density fitting with a standard TZVP auxiliary basis set[66]) to speed up the computations. Cartesian coordinates of the optimized structures are available in the Supporting Information (Table S5).

(50) Frisch, M. J.; Trucks, G. W.; Schlegel, H. B.; Scuseria, G. E.; Robb, M. A.; Cheeseman, J. R.; Montgomery, J. A., Jr.; Vreven, T.; Kudin, K. N.; Burant, J. C.; Millam, J. M.; Iyengar, S. S.; Tomasi, J.; Barone, V.; Mennucci, B.; Cossi, M.; Scalmani, G.; Rega, N.; Petersson, G. A.; Nakatsuji, H.; Hada, M.; Ehara, M.; Toyota, K.; Fukuda, R.; Hasegawa, J.; Ishida, M.; Nakajima, T.; Honda, Y.; Kitao, O.; Nakai, H.; Klene, M.; Li, X.; Knox, J. E.; Hratchian, H. P.; Cross, J. B.; Bakken, V.; Adamo, C.; Jaramillo, J.; Gomperts, R.; Stratmann, R. E.; Yazyev, O.; Austin, A. J.; Cammi, R.; Pomelli, C.; Ochterski, J. W.; Ayala, P. Y.; Morokuma, K.; Voth, G. A.; Salvador, P.; Dannenberg, J. J.; Zakrzewski, V. G.; Dapprich, S.; Daniels, A. D.; Strain, M. C.; Farkas, O.; Malick, D. K.; Rabuck, A. D.; Raghavachari, K.; Foresman, J. B.; Ortiz, J. V.; Cui, Q.; Baboul, A. G.; Clifford, S.; Cioslowski, J.; Stefanov, B. B.; Liu, G.; Liashenko, A.; Piskorz, P.; Komaromi, I.; Martin, R. L.; Fox, D. J.; Keith, T.; Al-Laham, M. A.; Peng, C. Y.; Nanayakkara, A.; Challacombe, M.; Gill, P. M. W.; Johnson, B.; Chen, W.; Wong, M. W.; Gonzalez, C.; Pople, J. A.; *Gaussian 03*, revision C.02; Gaussian, Inc.: Wallingford CT, 2004.
(51) Ahlrichs, R.; May, K. *Phys. Chem. Chem. Phys.* **2000**, *2*, 943.
(52) Kutzelnigg, W.; Fleischer, U.; Schindler, M. The IGLO-Method: Ab Initio Calculation and Interpretation of NMR Chemical Shifts and Magnetic Susceptibilities. In *NMR Basic Principles and Progress*; Diehl, P., Fluck, E., Günther, H., Kosfeld, R., Seelig, J., Eds.; Springer-Verlag: Berlin/Heidelberg, 1991; Vol. 23, p 165.
(53) Vosko, S. H.; Wilk, L.; Nusair, M. *Can. J. Phys.* **1980**, *58*, 1200.
(54) Becke, A. D. *Phys. Rev. A* **1988**, *38*, 3098.
(55) Perdew, J. P.; Wang, Y. *Phys. Rev. B: Condens. Matter Mater. Phys.* **1986**, *33*, 8822.
(56) Perdew, J. P.; Wang, Y. *Phys. Rev. B: Condens. Matter Mater. Phys.* **1986**, *34*, 7406.
(57) Becke, A. D. *J. Chem. Phys.* **1993**, *98*, 1372.
(58) Becke, A. D. *J. Chem. Phys.* **1993**, *98*, 5648.
(59) Perdew, J. P. *Physica B* **1991**, *172*, 1.
(60) Perdew, J. P.; Wang, Y. *Phys. Rev. B: Condens. Matter Mater. Phys.* **1992**, *45*, 13244.
(61) Hess, B. A.; Marian, C. M.; Wahlgren, U.; Gropen, O. *Chem. Phys. Lett.* **1996**, *251*, 365.
(62) Schimmelpfennig, B. *AMFI, Atomic Spin-Orbit Mean-Field Integral Program;* Stockholms Universitet: Stockholm, Sweden, 1996.
(63) Ahlrichs, R.; Bär, M.; Baron, H.; Bauernschmitt, R.; Böcker, S.; Deglmann, P.; Ehrig, M.; Eichkorn, K.; Elliott, S.; Furche, F.; Haase, F.; Häser, M.; Horn, H.; Hättig, C.; Huber, C.; Huniar, U.; Kattannek, M.; Köhn, A.; Kölmel, C.; Kollwitz, M.; May, K.; Ochsenfeld, C.; Öhm, H.; Schäfer, A.; Schneider, U.; Sierka, M.; Treutler, O.; Unterreiner, B.; von Arnim, M.; Weigend, F.; Weis, P.; Weiss, H. *Turbomole*, version 5.6; Quantum Chemistry Group, University of Karlsruhe: Karlsruhe, Germany, 2002.
(64) Andrae, D.; Häussermann, U.; Dolg, M.; Stoll, H.; Preuss, H. *Theor. Chim. Acta* **1990**, *77*, 123.
(65) Schäfer, A.; Huber, C.; Ahlrichs, R. *J. Chem. Phys.* **1994**, *100*, 5829.
(66) Eichkorn, K.; Treutler, O.; Öhm, H.; Häser, M.; Ahlrichs, R. *Chem. Phys. Lett.* **1995**, *242*, 652.
(67) Eichkorn, K.; Weigend, F.; Treutler, O.; Ahlrichs, R. *Theor. Chem. Acc.* **1997**, *97*, 119.

Agreement between optimized and experimental structures (where available) was generally good.

Note that we rely on the assumption that the coordination state of the complex present in the EPR experiments is generally equivalent to that characterized structurally, e.g., by X-ray diffraction. This is important, as even weakly coordinated solvent molecules may alter the spectral parameters substantially (see, for example, ref 68).

3. Results and Discussion

Here, we extend the validation study for EPR parameters of small and medium-sized molybdenum systems in paper I[23] to a number of larger Mo^V complexes (Figure 1) that are considered structural and spectroscopic models for molybdenum binding sites in proteins. On one hand, we want to be able to draw some reliable conclusions about the best methodology for such calculations by establishing the errors arising from (a) inaccuracies or approximations within the theoretical approach itself and (b) neglected environmental or dynamical effects. On the other hand, we intend to provide some insights relevant for understanding the EPR parameters of molybdoenzymes. As in paper I,[23] the importance of the exchange-correlation functional (in particular of exact-exchange admixture) and of SO coupling corrections to the HFC tensor are analyzed.

The Mo^V model complexes (Figure 1) can be divided into several subgroups that will be examined in turn. The first group includes $MoOOHL^1$, $MoOSHL^1$, and $MoOSEtL^1$, i.e., species with a terminal oxo ligand and an additional single-bonded oxygen- or sulfur-containing ligand that can in principle take different orientations of the hydrogen atom or ethyl chain. $MoOClL^1$ is similar except that it lacks this conformational freedom. The next group consists of two complexes with the L = tris-(3,5-dimethylpyrazolyl)hydroborate anion ligand: MoOLbdt and the cationic $[MoOLS_2CNEt_2]^+$. Similar to the former of these two complexes, the anionic $[MoOCl_2dtMe_2]^-$ exhibits a dithiolene chelate ligand, analogous to the biologically relevant molybdopterin. The final group contains anionic complexes with two terminal oxo ligands or one terminal oxo and one terminal sulfido ligand: $[MoO_2L^1]^-$, $[MoO_2L^2]^-$, and $[MoOSL^1]^-$. The difference between L^1 and L^2 is that L^1 possesses two nitrogen and two sulfur atoms to coordinate the metal whereas in L^2 sulfur is replaced by oxygen (cf. Figure 1). This group will be discussed last, as its EPR parameters differ notably from those of the other complexes.

General Trends and Observations. Before separately discussing these subgroups of complexes below, let us look at the general influence of the exchange-correlation functional and of SO corrections to HFC tensors on the agreement between theory and experiment. Tables 1 and 2 display the computed *g* and HFC tensors (in most cases with SO corrections), respectively, and Table 3 contains information about the relative tensor orientations. Further useful data is available in Supporting Information (Figure S1 shows spin density plots for some of the Mo^V compounds; Figure S2 displays SOMO plots for selected complexes; *g*-tensor orientations for some model complexes are depicted in Figure S3; Figures S4−S8 show MO schemes and a detailed *g*-tensor MO analysis for different compounds; Tables S1−S4 display analyses of atomic SO and MO contributions to the *g* tensors and to the SO correction of the HFC tensors, as well as Mulliken spin populations for selected complexes).

Starting with the *g* tensors (Table 1), we note that all systems exhibit two "perpendicular" components Δg_{22} and Δg_{33} with appreciably negative values (Δg_{33} is particularly negative for the last subset of complexes, with two terminal oxo and/or sulfido ligands) and one "parallel" component, Δg_{11}, that is either less negative or positive. This approximates the situation one would expect for a regular square-pyramidal coordination (cf., e.g., paper I for better examples of that type[23]). With the striking exception (to be discussed further below) of the Δg_{11} component for the last subset ($[MoO_2L^1]^-$, $[MoO_2L^2]^-$, and $[MoOSL^1]^-$), increasing HF exchange admixture renders all three tensor components more negative (less positive). We see that Δg_{22} and Δg_{33} are well-reproduced in most cases by a HF exchange admixture of ca. 30−40%. A notable exception is the very negative Δg_{33} component in the last subset, which is overshot (too negative) at this level, and its experimental value is already reached at 20% HF exchange (B3PW91). As found in paper I,[23] Δg_{11} is in most cases insufficiently negative or too positive at the corresponding levels, due to the neglect of higher-order SO contributions in the second-order perturbation *g*-tensor treatment (exceptions are $[MoOLS_2CNEt_2]^+$ and $[MoOCl_2dtMe_2]^-$, where larger exact-exchange admixtures actually bring g_{11} slightly below experiment). For this reason, the *g*-tensor anisotropy (cf. Table 1) is always overestimated by the calculations (except for $[MoOCl_2dtMe_2]^-$, where the computed Δg_{33} is not negative enough), whereas the *g*-tensor rhombicity is often reproduced reasonably well. The dependence of the anisotropy and rhombicity of the *g* tensor on the density functional is usually moderate. As spin-polarized two-component calculations, which provide the higher-order SO contributions to Δg_{11},[23] may currently be too computationally demanding to be applied routinely to realistic models of molybdoenzymes, one might also correct Δg_{11} based on experience[23] for smaller model complexes. However, given that the deviations from experiment for g_{11} at a given amount of exact-exchange admixture are not fully systematic (Table 1), more work clearly remains to be done.

Turning to the HFC tensors (Table 2), we see that negative spin density at the nucleus, deriving mostly from core−shell spin polarization, leads to positive A_{FC} values (due to the negative nuclear *g* factor of ^{95}Mo). As for the models studied in paper I,[23] A_{FC} is underestimated at the GGA level and increases with larger exact-exchange admixture. The first-order dipolar terms T_{ii} depend less on spin polarization and thus on the exchange-correlation functional.[34,35] The second-order SO corrections are in all cases very important for an accurate prediction of the isotropic couplings and also for the anisotropic part of the tensor. Their magnitude increases also with increasing exact-exchange admixture, in agreement with our findings in paper I.[23] At around 40% HF exchange

(68) Garner, C. D.; Hill, L. H.; Mabbs, F. E.; McFadden, D. L.; McPhail, A. T. *J. Chem. Soc., Dalton Trans.* **1977**, 1202.

Table 1. Dependence of *g*-Tensor Principal Values on the Choice of the Density Functional for the Mo^V Model Complexes[a]

complex	functional	g_{11}	g_{22}	g_{33}	Δg_{11}	Δg_{22}	Δg_{33}	$\Delta g_{11}-\Delta g_{33}$[b]	$(\Delta g_{11}-\Delta g_{22})/(\Delta g_{11}-\Delta g_{33})$[c]	$<S^2>$
MoOOHL[1]	SVWN5	2.0057	1.9689	1.9549	3421	−33410	−47388	51	0.72	0.7532
	BP86	2.0057	1.9719	1.9588	3353	−30405	−43514	47	0.72	0.7543
	B3PW91	1.9987	1.9646	1.9509	−3657	−37759	−51431	48	0.71	0.7585
	BPW91-30HF	1.9941	1.9611	1.9472	−8190	−41217	−55129	47	0.70	0.7623
	BPW91-40HF	1.9890	1.9570	1.9424	−13316	−45309	−59911	47	0.68	0.7676
	BPW91-50HF	1.9833	1.9528	1.9367	−19014	−49560	−65647	47	0.66	0.7760
	exp[17]	1.9805(4)	1.9470(4)	1.9438(4)	−21819	−55319	−58519	37	0.91	
MoOSHL[1]	SVWN5	2.0379	1.9717	1.9723	35611	−30610	−30017	66	0.99	0.7534
	BP86	2.0355	1.9736	1.9743	33191	−28766	−28024	62	0.99	0.7546
	B3PW91	2.0309	1.9663	1.9630	28607	−36031	−39364	68	0.95	0.7592
	BPW91-30HF	2.0284	1.9627	1.9587	26042	−39669	−43612	70	0.94	0.7634
	BPW91-40HF	2.0249	1.9584	1.9534	22536	−43957	−48891	71	0.93	0.7688
	BPW91-50HF	2.0202	1.9535	1.9474	17841	−48774	−54928	73	0.92	0.7774
	exp[17]	2.0155(4)	1.9598(4)	1.9523(4)	13181	−42519	−50019	63	0.88	
MoOSEtL[1]	SVWN5	2.0391	1.9742	1.9588	36755	−28129	−43515	80	0.81	0.7529
	BP86	2.0367	1.9758	1.9616	34349	−26554	−40673	75	0.81	0.7541
	B3PW91	2.0372	1.9693	1.9537	34926	−32977	−48582	84	0.81	0.7583
	BPW91-30HF	2.0344	1.9651	1.9496	32110	−37236	−52687	85	0.82	0.7621
	BPW91-40HF	2.0318	1.9610	1.9445	29452	−41295	−57773	87	0.81	0.7668
	exp[18]	2.024(1)	1.964(1)	1.955(1)	21681	−38319	−47319	69	0.87	
MoOClL[1]	SVWN5	2.0264	1.9629	1.9457	24047	−39387	−56589	81	0.79	0.7530
	BP86	2.0262	1.9663	1.9524	23924	−36031	−49889	74	0.81	0.7540
	B3PW91	2.0225	1.9598	1.9455	20229	−42483	−56834	77	0.81	0.7584
	BPW91-30HF	2.0192	1.9567	1.9429	16921	−45643	−59454	76	0.82	0.7626
	BPW91-40HF	2.0149	1.9525	1.9392	12606	−49806	−63074	76	0.82	0.7681
	BP86[21]	2.0210	1.9640	1.9500	18681	−38319	−52319	71	0.80	
	exp[20]	2.007	1.960	1.949	4680	−42320	−53320	58	0.81	
MoOLbdt	SVWN5	2.0169	1.9806	1.9296	14618	−21690	−72683	87	0.42	0.7523
	BP86	2.0157	1.9811	1.9341	13423	−21225	−68269	82	0.42	0.7536
	B3PW91	2.0152	1.9726	1.9250	12904	−29761	−77358	90	0.47	0.7583
	BPW91-30HF	2.0109	1.9676	1.9217	8604	−34691	−80605	89	0.49	0.7629
	BPW91-40HF	2.0073	1.9627	1.9178	4951	−39593	−84501	89	0.50	0.7695
	exp[19]	2.004(1)	1.972(1)	1.934(1)	1681	−30319	−68319	70	0.46	
$[MoOLS_2CNEt_2]^+$	SVWN5	1.9934	1.9768	1.9621	−8871	−25565	−40180	31	0.53	0.7541
	BP86	1.9926	1.9782	1.9641	−9747	−24161	−38181	28	0.51	0.7556
	B3PW91	1.9870	1.9747	1.9589	−15273	−27583	−43423	28	0.44	0.7620
	BPW91-30HF	1.9796	1.9670	1.9491	−22759	−35279	−53222	30	0.41	0.7689
	BPW91-40HF	1.9739	1.9622	1.9437	−28385	−40132	−58581	30	0.39	0.7799
	exp[19]	1.980(1)	1.970(1)	1.954(1)	−22319	−32319	−48319	26	0.38	
$[MoOCl_2dtMe_2]^-$	SVWN5	2.0234	1.9767	1.9721	21041	−25606	−30215	51	0.91	0.7537
	BP86	2.0211	1.9778	1.9734	18746	−24566	−28961	48	0.91	0.7548
	B3PW91	2.0134	1.9713	1.9657	11061	−31049	−36609	48	0.88	0.7583
	BPW91-30HF	2.0088	1.9679	1.9619	6503	−34375	−40429	47	0.87	0.7611
	BPW91-40HF	2.0041	1.9640	1.9574	1799	−38272	−44952	47	0.86	0.7644
	BPW91-50HF	1.9993	1.9596	1.9523	−3061	−42687	−50048	47	0.84	0.7689
	BPW91-60HF	1.9943	1.9545	1.9464	−8006	−47822	−55918	48	0.83	0.7753
	exp[22]	2.004	1.967	1.943	1681	−35319	−59319	61	0.61	
$[MoO_2L^2]^-$	SVWN5	2.0056	1.9331	1.7722	3313	−69228	−230085	233	0.31	0.7515
	BP86	2.0054	1.9426	1.8033	3034	−59688	−199029	202	0.31	0.7519
	B3PW91	2.0071	1.9295	1.7522	4783	−72779	−250137	255	0.30	0.7527
	BPW91-30HF	2.0084	1.9246	1.7299	6057	−77716	−272385	278	0.30	0.7536
	BPW91-40HF	2.0101	1.9182	1.7019	7790	−84111	−300415	308	0.30	0.7548
	exp[16]	1.979	1.897	1.754	−23319	−105319	−248319	225	0.36	
$[MoO_2L^1]^-$	SVWN5	2.0085	1.9439	1.8322	6219	−58373	−170130	176	0.37	0.7514
	BP86	2.0081	1.9513	1.8537	5767	−51033	−148590	154	0.36	0.7519
	B3PW91	2.0105	1.9376	1.8068	8179	−64766	−195532	204	0.36	0.7544
	BPW91-30HF	2.0125	1.9320	1.7856	10132	−70368	−216758	227	0.35	0.7570
	BPW91-40HF	2.0153	1.9250	1.7601	12989	−77330	−242198	255	0.35	0.7608
	BPW91-50HF	2.0194	1.9176	1.7338	17051	−84769	−268565	286	0.36	0.7667
	exp[17]	1.9868(4)	1.9158(4)	1.8106(4)	−15519	−86519	−191719	176	0.40	
[$MoOSL^1]^-$	SVWN5	2.0338	1.9345	1.8539	31447	−67848	−148405	180	0.55	0.7526
	BP86	2.0343	1.9461	1.8800	31929	−56175	−122294	154	0.57	0.7539
	B3PW91	2.0411	1.9429	1.8689	38809	−59401	−133418	172	0.57	0.7593
	BPW91-30HF	2.0454	1.9428	1.8656	43053	−59511	−136770	180	0.57	0.7635
	BPW91-40HF	2.0513	1.9420	1.8592	49006	−60343	−143124	192	0.57	0.7682
	BPW91-50HF	2.0593	1.9417	1.8519	57007	−60619	−150411	207	0.57	0.7741
	exp[17]	2.0165(4)	1.9336(4)	1.8885(4)	14181	−68719	−113819	128	0.65	

[a] All computations were performed using the 12s6p5d basis set for molybdenum and the IGLO-II basis sets for all other atoms. The *g* shifts (Δg) are given in ppm, and the *g* anisotropy is given in ppt. The error of the experimental *g* shifts is ±400 or ±1000 ppm (cf. error of g_{ii} values given in the table). [b] *g* Anisotropy = $\Delta g_{11} - \Delta g_{33}$ in ppt. [c] *g*-Tensor rhombicity = $(\Delta g_{11} - \Delta g_{22})/(\Delta g_{11} - \Delta g_{33})$.

Table 2. Dependence of HFC Constants on the Choice of the Density Functional for the Mo^V Model Complexes[a]

complex	functional	A_{FC}	A_{PC}	A'_{iso}[b]	T_{11}	T_{22}	T_{33}	$T_{11,orb}$	$T_{22,orb}$	$T_{33,orb}$	T'_{11}[c]	T'_{22}[c]	T'_{33}[c]	$<S^2>$
MoOOHL[1]	SVWN5	45.2	11.5	56.7	58.0	−31.8	−26.1	4.4	−3.3	−1.2	62.0	−34.7	−27.4	0.7532
	BP86	56.3	11.1	67.4	57.6	−31.4	−26.2	4.3	−3.1	−1.2	61.6	−34.2	−27.4	0.7543
	B3PW91	74.9	13.4	88.3	62.9	−33.9	−29.0	5.2	−3.5	−1.6	67.6	−37.0	−30.5	0.7585
	BPW91-30HF	85.8			64.7	−34.8	−29.9							0.7623
	BPW91-40HF	94.7	15.2	109.9	66.5	−35.9	−30.6	6.5	−4.3	−2.2	72.4	−39.7	−32.7	0.7676
	BPW91-50HF	103.9			68.1	−37.2	−31.0							0.7760
	exp[17]			117.5(6)							74.3(7)	−30.6(7)	−44.1(7)	
MoOSHL[1]	SVWN5	42.8	8.8	51.6	51.9	−27.3	−24.6	2.7	−1.6	−1.1	54.1	−28.5	−25.6	0.7534
	BP86	50.9	8.7	59.6	51.7	−27.2	−24.5	2.6	−1.5	−1.1	53.9	−28.4	−25.5	0.7546
	B3PW91	68.2	10.6	78.8	57.3	−30.2	−27.1	3.4	−1.9	−1.5	60.0	−31.7	−28.2	0.7592
	BPW91-30HF	78.5			59.7	−31.5	−28.2							0.7634
	BPW91-40HF	87.4	12.7	100.1	62.0	−32.9	−29.1	4.3	−2.3	−2.0	65.4	−34.9	−30.5	0.7688
	BPW91-50HF	96.5			64.3	−34.3	−30.0							0.7774
	exp[17]			102.2(6)							51.0(7)	−33.0(7)	−32.4(7)	
MoOSEtL[1]	SVWN5	40.7	8.7	49.4	49.6	−27.7	−21.9	3.2	−1.7	−1.4	51.5	−29.2	−22.3	0.7529
	BP86	48.4	8.6	57.0	49.6	−27.5	−22.1	3.0	−1.6	−1.4	51.6	−29.0	−22.6	0.7541
	B3PW91	65.2			55.3	−30.2	−25.1							0.7583
	BPW91-30HF	75.3			57.7	−31.4	−26.3							0.7621
	BPW91-40HF	84.0	12.5	96.5	60.1	−32.6	−27.5	4.5	−2.5	−2.0	63.0	−34.7	−28.3	0.7668
	exp[18]			104(3)							71(4)	−33(4)	−37(4)	
MoOClL[1]	SVWN5	46.5	12.0	58.5	53.2	−27.7	−25.5	3.4	−2.7	−0.7	55.5	−30.1	−25.3	0.7530
	BP86	56.0	11.4	67.4	53.0	−27.7	−25.3	3.1	−2.5	−0.7	55.4	−30.0	−25.4	0.7540
	B3PW91	74.2	13.1	87.3	58.3	−30.6	−27.7	3.9	−2.9	−1.0	61.4	−33.2	−28.1	0.7584
	BPW91-30HF	85.4			60.5	−31.8	−28.7							0.7626
	BPW91-40HF	95.0	15.0	110.0	62.7	−33.0	−29.8	4.9	−3.4	−1.5	66.8	−36.1	−30.7	0.7681
	BP86[21]			61.3							50.6	−25.3	−25.3	
	exp[20]			107							61			
	exp[21]			98							66	−35	−31	
MoOLbdt	SVWN5	42.6	8.8	51.4	48.8	−19.7	−29.1	6.3	−1.6	−4.8	54.2	−21.3	−32.9	0.7523
	BP86	52.1	8.8	60.9	50.0	−20.7	−29.3	6.2	−1.6	−4.6	55.3	−22.3	−33.1	0.7536
	B3PW91	70.3			57.7	−25.7	−32.0							0.7583
	BPW91-30HF	82.8			61.3	−28.4	−32.9							0.7629
	BPW91-40HF	92.4	13.5	105.9	63.6	−30.3	−33.4	8.1	−2.9	−5.2	70.5	−33.2	−37.3	0.7695
	exp[19]			111(3)							39(4)	−77(4)	38(4)	
	own simulation[d]			114							64	−30	−33	
$[MoOLS_2CNEt_2]^+$	SVWN5	44.4	9.9	54.3	58.2	−31.8	−26.4	4.8	−3.1	−1.7	62.5	−34.9	−27.5	0.7541
	BP86	56.0	9.9	65.9	58.1	−31.5	−26.5	4.8	−3.1	−1.7	62.4	−34.7	−27.7	0.7556
	B3PW91	76.3			63.6	−34.2	−29.4							0.7620
	BPW91-30HF	88.3			64.9	−34.7	−30.2							0.7689
	BPW91-40HF	98.6	14.4	113.0	66.0	−35.2	−30.8	6.5	−4.6	−1.9	72.2	−39.8	−32.5	0.7799
	exp[19]			108(3)							85(4)	−18(4)	−67(4)	
	own simulation[d]			123							70	−38	−33	
$[MoOCl_2dtMe_2]^-$	SVWN5	48.3	10.3	58.6	59.1	−29.4	−29.7	4.1	−1.9	−2.2	62.9	−31.3	−31.6	0.7537
	BP86	59.1	10.2	69.3	58.5	−29.1	−29.4	4.0	−1.8	−2.2	62.2	−31.0	−31.3	0.7548
	B3PW91	77.1	11.9	89.0	63.4	−31.6	−31.9	4.8	−2.2	−2.6	67.9	−33.7	−34.2	0.7583
	BPW91-30HF	87.8	12.8	100.6	65.2	−32.4	−32.8	5.2	−2.3	−2.9	70.1	−34.8	−35.3	0.7611
	BPW91-40HF	96.6	13.7	110.3	67.2	−33.5	−33.7	5.6	−2.5	−3.1	72.5	−35.9	−36.5	0.7644
	BPW91-50HF	105.3	14.7	120.0	69.1	−34.5	−34.6	6.0	−2.7	−3.3	74.8	−37.0	−37.8	0.7689
	BPW91-60HF	114.1	15.7	129.8	71.0	−35.5	−35.6	6.4	−2.9	−3.5	77.1	−38.1	−39.0	0.7753
	exp[22]			118							62	−73	11	
	own simulation[d]			112							74	−37	−37	
$[MoO_2L^2]^-$	SVWN5	60.1	23.5	83.6	−29.7	−28.7	58.4	−18.8	−6.3	25.1	−48.5	−35.0	83.5	0.7515
	BP86	74.8	21.0	95.8	−30.0	−28.4	58.4	−16.2	−5.8	22.0	−46.2	−34.2	80.4	0.7519
	B3PW91	97.9			−34.1	−29.8	64.0							0.7527
	BPW91-30HF	110.4			−35.7	−29.9	65.6							0.7536
	BPW91-40HF	120.4	28.5	148.9	−37.4	−30.1	67.4	−23.7	−8.9	32.6	−61.0	−39.0	100.0	0.7548
	exp[16]													
$[MoO_2L^1]^-$	SVWN5	47.7	19.3	67.0	−26.4	−25.7	52.0	−15.4	−5.0	20.3	−41.7	−30.6	72.3	0.7514
	BP86	58.2	17.5	75.7	−26.7	−25.5	52.2	−13.4	−4.6	17.9	−40.1	−30.0	70.1	0.7519
	B3PW91	78.9	20.2	99.1	−31.3	−26.6	57.8	−15.6	−5.2	20.2	−46.9	−31.7	78.0	0.7544
	BPW91-30HF	89.8			−33.3	−26.4	59.7							0.7570
	BPW91-40HF	98.5	24.5	123.1	−35.3	−26.2	61.5	−20.9	−6.9	27.8	−56.2	−33.0	89.2	0.7608
	BPW91-50HF	106.9			−37.4	−25.7	63.2							0.7667
	exp[17]			127.1(6)							−45.9(6)	−33.6(6)	79.1(8)	
$[MoOSL^1]^-$	SVWN5	38.4	16.9	55.3	43.4	−20.6	−22.8	12.9	−1.3	−11.5	51.9	−22.8	−29.1	0.7526
	BP86	45.7	14.8	60.5	43.3	−20.7	−22.6	10.9	−1.4	−9.5	50.7	−22.8	−27.9	0.7539
	B3PW91	60.5	17.8	78.3	45.8	−22.3	−23.5	13.6	−1.7	−12.1	54.8	−24.4	−31.1	0.7593
	BPW91-30HF	68.3			46.1	−22.5	−23.6							0.7635
	BPW91-40HF	74.1	16.9	91.0	46.0	−22.5	−23.4	14.0	−3.0	−11.1	55.5	−25.8	−29.7	0.7682
	BPW91-50HF	78.7			45.1	−22.1	−23.0							0.7741
	exp[17]			99.5(9)							61(1)	−29.1(9)	−31.7(9)	

[a] First-order HFC constants (A_{FC} and T_{ii}), second-order SO correction terms (A_{PC} and $T_{ii,orb}$) as well as the total HFCs (A'_{iso} and T'_{ii}) are shown (in MHz). Spin−orbit corrections to the HFC values have not been obtained with all functionals. The T_{ii}, $T_{ii,orb}$, and T'_{ii} values are given as eigenvalues of the corresponding tensors, i.e., in their own principal axis systems. All computations were performed using the 12s6p5d basis set for molybdenum and the IGLO-II basis sets for all other atoms. [b] $A'_{iso} = A_{FC} + A_{PC}$. [c] $T'_{ii} = T_{ii} + T_{ii,orb}$. This sum relation is only valid if the principal axis systems of all three tensors coincide. Since this is not the case for less-symmetrical compounds, T'_{ii} will in general deviate from the sum of the two eigenvalues T_{ii} and $T_{ii,orb}$. The size of this deviation is an indicator of how much the axis systems differ from each other. [d] For a description see also the text and the Supporting Information. The *g* values were taken from the original references for all simulations.

Table 3. Relative Orientations of g and HFC Tensors for the Mo^V Model Complexes Expressed in Terms of the Angles (deg) between the Axes of the g and A Principal Axis Systems[a]

		computed orientation			experimental orientation		
complex		A_{11}	A_{22}	A_{33}	A_{11}	A_{22}	A_{33}
MoOOHL[1]							
	g_{11}	5.3	90.4	84.8	26(1)[b]	90	64
BP86	g_{22}	88.9	7.8	97.7	90	0	90
	g_{33}	95.1	82.2	9.4	116	90	26(1)
		$\alpha = -55.9$	$\beta = 9.4$	$\gamma = 56.6$	$\alpha = 0$	$\beta = 26$	$\gamma = 0$
	g_{11}	6.0	91.3	84.2			
+SO−HFC corr	g_{22}	88.3	3.9	93.5			
	g_{33}	95.8	86.4	6.8			
		$\alpha = -30.9$	$\beta = 6.8$	$\gamma = 32.4$			
	g_{11}	14.6	95.0	76.4			
BPW91-40HF	g_{22}	83.3	9.3	96.4			
	g_{33}	102.9	82.2	15.1			
		$\alpha = -25.3$	$\beta = 15.1$	$\gamma = 31.3$			
	g_{11}	15.8	96.7	75.7			
+SO−HFC corr	g_{22}	82.7	7.5	91.7			
	g_{33}	103.9	86.5	14.4			
		$\alpha = -6.9$	$\beta = 14.4$	$\gamma = 14.1$			
MoOSHL[1]							
	g_{11}	43.6	77.1	49.3	16(1)[b]	90	74
BP86	g_{22}	97.9	13.1	100.4	90	0	90
	g_{33}	132.5	87.6	42.6	106	90	16(1)
		$\alpha = -15.5$	$\beta = 42.6$	$\gamma = 3.5$	$\alpha = 0$	$\beta = 16$	$\gamma = 0$
	g_{11}	44.5	75.5	49.1			
+SO−HFC corr	g_{22}	97.8	15.0	102.7			
	g_{33}	133.5	86.1	43.7			
		$\alpha = -18.6$	$\beta = 43.7$	$\gamma = 5.7$			
	g_{11}	7.1	95.4	94.6			
B3PW91	g_{22}	86.0	16.6	106.1			
	g_{33}	84.1	74.4	16.7			
		$\alpha = -106.1$	$\beta = 16.7$	$\gamma = 110.8$			
	g_{11}	6.1	92.4	84.4			
BPW91-40HF	g_{22}	86.8	8.5	97.9			
	g_{33}	95.2	81.8	9.7			
		$\alpha = -54.8$	$\beta = 9.7$	$\gamma = 57.6$			
	g_{11}	7.3	92.2	83.0			
+SO−HFC corr	g_{22}	86.8	9.0	98.4			
	g_{33}	96.6	81.3	11.0			
		$\alpha = -50.2$	$\beta = 11.0$	$\gamma = 53.0$			
MoOSEtL[1]							
	g_{11}	16.3	103.8	81.4	24(2)[b]	90	66
BPW91-40HF	g_{22}	78.2	17.0	78.0	90	0	90
	g_{33}	101.1	99.7	14.8	114	90	24(2)
		$\alpha = 54.3$	$\beta = 14.8$	$\gamma = -41.3$	$\alpha = 0$	$\beta = 24$	$\gamma = 0$
MoOClL[1]							
	g_{11}	5.9	86.7	85.1			
BPW91-40HF	g_{22}	94.7	19.8	70.8			
	g_{33}	93.5	109.5	19.8			
		$\alpha = 75.4$	$\beta = 19.8$	$\gamma = -79.5$			
	g_{11}	7.1	85.8	84.3			
+SO−HFC corr	g_{22}	95.3	12.3	78.9			
	g_{33}	94.8	101.6	12.6			
		$\alpha = 62.6$	$\beta = 12.6$	$\gamma = -67.3$			
MoOLbdt							
	g_{11}	59.3	89.9	30.7	45[c]/0(2)[b]	90	45/90
BP86	g_{22}	90.0	0.1	90.1	90	0	90
	g_{33}	149.3	90.0	59.3	135/90	90	45/0(2)
		$\alpha = -0.1$	$\beta = 59.3$	$\gamma = 0.0$	$\alpha = 0$	$\beta = 45/0$	$\gamma = 0$
	g_{11}	61.3	89.9	28.7			
+SO−HFC corr	g_{22}	90.0	0.1	90.1			
	g_{33}	151.3	90.0	61.3			
		$\alpha = -0.1$	$\beta = 61.3$	$\gamma = 0.0$			
	g_{11}	51.8	90.0	38.2			
BPW91-40HF	g_{22}	90.0	0.0	90.0			
	g_{33}	141.8	90.0	51.8			
		$\alpha = 0.0$	$\beta = 51.8$	$\gamma = 0.0$			
	g_{11}	54.1	90.0	35.9			
+SO−HFC corr	g_{22}	90.0	0.0	90.0			
	g_{33}	144.1	90.0	54.1			
		$\alpha = 0.0$	$\beta = 54.1$	$\gamma = 0.0$			

Table 3. Continued

complex		computed orientation A_{11}	A_{22}	A_{33}	experimental orientation A_{11}	A_{22}	A_{33}
$[MoOLS_2CNEt_2]^+$							
	g_{11}	33.7	89.8	56.3	36(2)[b,c]	90	54
BPW91-40HF	g_{22}	89.9	0.5	90.5	90	0	90
	g_{33}	123.7	89.5	33.7	126	90	36(2)
		$\alpha = -0.9$	$\beta = 33.7$	$\gamma = 0.8$	$\alpha = 0$	$\beta = 36$	$\gamma = 0$
$[MoOCl_2dtMe_2]^-$							
	g_{11}	16.9	89.4	106.9	22[c]	90	68
BPW91-40HF	g_{22}	90.2	1.3	88.7	90	0	90
	g_{33}	73.1	91.2	16.9	112	90	22
		$\alpha = 175.5$	$\beta = 16.9$	$\gamma = -175.9$	$\alpha = 0$	$\beta = 22$	$\gamma = 0$
	g_{11}	17.7	90.1	107.7			
+SO−HFC corr	g_{22}	90.2	1.0	91.0			
	g_{33}	72.3	89.0	17.7			
		$\alpha = -176.8$	$\beta = 17.7$	$\gamma = 176.8$			
$[MoO_2L^2]^-$							
	g_{11}	1.0	89.0	90.3			
BPW91-40HF	g_{22}	91.0	1.8	88.5			
	g_{33}	89.7	91.5	1.5			
		$\alpha = 99.8$	$\beta = 1.5$	$\gamma = -100.8$			
$[MoO_2L^1]^-$							
	g_{11}	0.4	90.4	89.8	0[b]	90	90
BPW91-40HF	g_{22}	89.6	3.1	87.0	90	0	90
	g_{33}	90.2	93.0	3.0	90	90	0
		$\alpha = 86.8$	$\beta = 3.0$	$\gamma = -86.4$	$\alpha = 0$	$\beta = 0$	$\gamma = 0$
	g_{11}	0.3	90.3	89.9			
+SO−HFC corr	g_{22}	89.8	2.2	87.9			
	g_{33}	90.1	92.1	2.1			
		$\alpha = 87.0$	$\beta = 2.1$	$\gamma = -86.7$			
$[MoOSL^1]^-$							
	g_{11}	37.2	70.7	59.5	36(1)[b]	90	54
BPW91-40HF	g_{22}	86.5	37.8	127.6	90	0	90
	g_{33}	127.0	58.9	52.5	126	90	36(1)
		$\alpha = -50.3$	$\beta = 52.5$	$\gamma = 40.7$	$\alpha = 0$	$\beta = 36$	$\gamma = 0$
	g_{11}	44.5	88.8	45.6			
+SO−HFC corr	g_{22}	86.2	6.8	95.6			
	g_{33}	134.2	83.3	45.0			
		$\alpha = -8.0$	$\beta = 45.0$	$\gamma = 9.5$			

[a] The eigenvectors of the two tensors are taken to span right-handed coordinate systems with an orientation of the axes in the molecular frame as shown exemplarily in Figure 2. Additionally, the corresponding Euler angles (defined as subsequent rotations around $z-y'-z''$ axes) are given. All computations were performed using the 12s6p5d basis set for molybdenum and the IGLO-II basis sets for all other atoms. All angles are given in degrees. [b] From original references (see also text and Table 1). [c] From own simulations (see also text and Supporting Information).

admixture, the isotropic pseudo-contact correction term A_{PC} typically amounts to 14−17% of the first-order Fermi contact term A_{FC} (A_{iso}). At the same level, the anisotropic orbital HFC correction term $T_{ii,orb}$ is around 5−16% of the first-order dipolar HFC term T_{ii} (Table 2). For the three systems with two terminal oxo and/or sulfido ligands ($[MoO_2L^1]^-$, $[MoO_2L^1]^-$, and $[MoOSL^1]^-$), contributions from the SO−HFC corrections are even more pronounced, for reasons that are related to the large g anisotropies (see below). In any case, it is clear that meaningful comparison with experiment for molybdoenzymes or model complexes requires the inclusion of SO corrections to the metal HFC parameters. We note in passing that earlier, more approximate calculations by Westmoreland and co-workers suggested a lower importance of second-order SO corrections to the metal hyperfine couplings.[37,69,70] In our comparison with experiment for A_{iso}, we should furthermore keep in mind the likely enhancement of A_{FC} of about 20% by scalar relativistic effects (see above and paper I[23]).

As a further, general observation, we note that even at relatively high exact-exchange admixtures, spin contamination of the Kohn−Sham wavefunction remains low for all systems studied here (Table 1). This suggests relatively little metal−ligand antibonding character of the SOMO.[34,35] This was also found for the systems in paper I, with one exception.[23]

A general problem for the validation of computed molybdenum HFC constants and HFC-tensor orientations with respect to the g-tensor principal axis system is the difficulty of finding precise and reliable experimental data. The reasons for this are (a) the low natural abundance of molybdenum nuclei with a nuclear spin $I > 0$ (^{95}Mo: 15.9%, ^{97}Mo: 9.6%; both with $I = {}^5/_2$) and (b) spectral overlap for continuous wave EPR spectra taken at S- or X-band microwave frequencies (roughly 3 and 9 GHz, respectively). It would thus be desirable to have experimental HFC tensors originating from multifrequency and/or high-frequency EPR studies employing $^{95/97}$Mo-enriched samples. However, in many cases the experimental work was carried out using solely X-band EPR spectroscopy on nonenriched samples. Therefore, the experimental HFC parameters and Euler

(69) Balagopalakrishna, C.; Kimbrough, J. T.; Westmoreland, T. D. *Inorg. Chem.* **1996**, *35*, 7758.
(70) Nipales, N. S.; Westmoreland, T. D. *Inorg. Chem.* **1997**, *36*, 756.

angles connecting the HFC with the *g* tensor may be less reliable for some of the complexes. Furthermore, as discussed already in paper I,[23] the availability of single-crystal EPR data, giving the orientation of the *g* and HFC tensors relative to the molecular frame, is very limited. Among the compounds investigated here, such information is only available for $MoOClL^1$.[21] As our calculations identified problems with the original simulations for some of the systems studied (see below), Table 2 includes revised "experimental" HFC data that were obtained by our own simulations, as will be detailed below.

Computed relative orientations of the HFC and *g* tensors (with respect to each other and to the molecular frame; cf. Table 3) will be discussed separately for each group of complexes (see below). For most of the complexes, the SO correction does not alter the relative orientation of the *g* and HFC tensors dramatically (changes are usually smaller than 7°; cf. Table 3), although there is also a case where SO−HFC corrections significantly influence the orientation of the HFC tensor with respect to the *g* tensor ($[MoOSL^1]^-$; cf. Table 3). The experimental HFC-tensor orientations may also be affected by problems with spectra simulation (see below), and they will in some cases be provided based on revised simulations.

$MoOOHL^1$, $MoOSHL^1$, and $MoOSEtL^1$. The complexes of this first group, which exhibit structural and spectroscopical similarities to the low-pH and high-pH forms of sulfite oxidase and the "very rapid" form of xanthine oxidase,[21] possess an oxygen- or sulfur-containing ligand (OH, SH, or SEt) which has some rotational freedom. That is, there may be different conformers with respect to the orientation of the hydrogen atoms or the ethyl chain. This ligand orientation might strongly influence some of the EPR parameters of the complex. Furthermore, the experimental values might be averaged values for an ensemble of different conformers. In our study, we consider only one (energy-minimized) conformer for each complex, except for $MoOOHL^1$, where we also performed one calculation for a different OH orientation (without further structure optimization) to test the sensitivity of the EPR parameters to such structural changes. The two complexes with sulfur ligands (SH and SEt) possess positive Δg_{11} shifts, and the g_{11} value of $MoOSEtL^1$ (2.024) is the highest *g* value of all complexes in this study (Table 1). $MoOOHL^1$ on the other hand exhibits a negative Δg_{11} shift, which is in accordance with the well-known trend that an exchange of an oxygen by a sulfur ligand in equatorial position leads to an increased average *g* value[37] (replacement of the axial oxo ligand by a sulfido ligand may actually *decrease* all *g*-tensor components[71]). This is usually attributed[37,69] to a more covalent metal−ligand bond and sometimes also to larger ligand SO contributions for the heavier ligand. Our own analyses for $MoOCl_4^-$ in paper I[23] and previous analyses[32] for $CrOF_4^-$ and $CrOCl_4^-$ have confirmed that both aspects are important. For example, on going from $CrOF_4^-$ to $CrOCl_4^-$, the magnitude of the metal SO contributions to $\Delta g_{||}$ is diminished from −25 000 to −11 000 ppm. This reflects the more covalent M−Cl bond compared with the the M−F bond and a consequent lower metal spin density. At the same time, the halogen SO contributions to the same component increase from +10 000 to +30 000 ppm.[32] The fact that even for 50% exact exchange the Δg_{11} shifts are still too positive may be attributed to the neglect of higher-order SO effects.[23] A similar trend holds also for Δg_{22} of $MoOOHL^1$, whereas the Δg_{22} components of the other two complexes and all Δg_{33} components are reproduced nicely at ca. 30−40% HF exchange admixture.

The HFC tensors for the three complexes follow the above-mentioned general behavior (increase of absolute values with exact-exchange admixture), including the overall reasonable agreement with experiment at the BPW91-40HF level (after the inclusion of SO corrections; Table 2). The largest deviations from experiment pertain to T_{11} for $MoOSHL^1$, which tends to be overestimated with the exact-exchange admixture (after the inclusion of SO corrections). Furthermore, for $MoOOHL^1$ and $MoOSEtL^1$, there seems to be a problem with the ordering of the T_{22} and T_{33} components. The calculations predict T_{22} to be larger than T_{33}, but the experimental values show an opposite order. It is not clear where this discrepancy comes from. But at least in the case of $MoOSEtL^1$ the experimental errors are quite large, rendering an unambiguous experimental discrimination difficult.

Simulations of frozen-solution EPR spectra of the three complexes of this subcategory yielded experimental relative tensor orientations that are quite similar: The g_{22} and A_{22} axes are collinear, and the $g_{11}-A_{11}$ and $g_{33}-A_{33}$ angles are 26°, 16°, and 24° for $MoOOHL^1$, $MoOSHL^1$, and $MoOSEtL^1$, respectively (Table 3).[17,18] Our computations, however, result in different tensor orientations. For all three complexes, the $g_{11}-A_{11}$ and $g_{33}-A_{33}$ angles are computed (BPW91-40HF) to be smaller than those found experimentally (by roughly 8−11°) and the calculated $g_{22}-A_{22}$ angle is always larger than zero. Thus, we find deviations from collinearity of the g_{22} and A_{22} axes of 9.3°, 8.5°, and 17.0°. SO corrections do not change this much: For $MoOOHL^1$ and $MoOSHL^1$, they give alterations of the BPW91-40HF angles of only about 1−2°. Figure 2 shows the computed *g*- and HFC-tensor principal axis systems for $MoOSHL^1$ in the molecular frame, illustrating the relative and absolute *g*- and HFC-tensor orientations (similar orientations hold for related compounds). The g_{11}/A_{11} axes lie almost along the Mo−O bond, the g_{22}/A_{22} axes are oriented toward one of the sulfur atoms of the tetradentate ligand, and the g_{33}/A_{33} axes point roughly in the direction of the SH group. For $MoOOHL^1$ and $MoOSHL^1$ tensor orientations from BP86 and B3PW91 calculations (the latter only for $MoOSHL^1$), are also listed in Table 3. The results clearly indicate that the angles can be substantially influenced by exact-exchange admixture. Especially for $MoOSHL^1$, the GGA results yield a very different tensor orientation than that obtained with the hybrid fuctional. In this case, mainly the *g*-tensor principal axes change their direction whereas the HFC-tensor axes remain almost constant in the different computations. For $MoOOHL^1$, the

(71) Young, C. G.; Collison, D.; Mabbs, F. E.; Enemark, J. H. *Inorg. Chem.* **1987**, *26*, 2925.

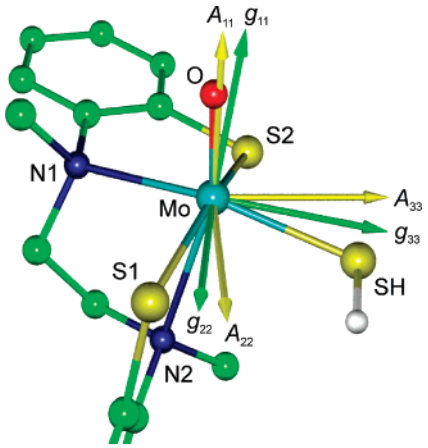

Figure 2. Computed orientation of the *g* (green) and HFC (yellow, including SO corrections to the tensor orientation) tensors in the molecular frame for MoOSHL[1] (BPW91-40HF results). Principal axis systems are taken to be right-handed coordinate systems. For the sake of clarity, hydrogen atoms (except for SH group) and parts of the lower phenyl ring (also cf. Figure 1) are omitted.

difference between the various methods is not so dramatic and here both tensors change their orientation (SO−HFC corrections are still inconsequential for the interaxial angles). At the moment, the reasons for the described discrepancies between theory and experiment are not clear. It could be that the experimental data are wrong (meaning that these simulation parameters are not a unique solution for simulating the EPR spectra) or that there is a problem with the calculations (in view of the general experience for such systems this is more likely with the molecular structure than with the computational method). Depending on the resolution of the EPR spectrum, it may not have been possible to unambiguously distinguish several very different sets of Euler angles (cf. examples below). Another possibility to explain the partial disagreement with experiment, especially concerning the tensor orientations, would be that the molecular structure used for the computations is not the same as the structure in frozen solution that was investigated by EPR spectroscopy. It might very well be that the orientation of the OH, SH, and SEt ligands is different from our equilibrium structures or that an ensemble of different conformations exists in solution.

To get an estimate of how an altered ligand orientation can influence the EPR parameters, we performed a calculation for MoOOHL[1] with changed orientation of the hydroxo ligand. The dihedral angle ∠(H−O−Mo−O) of 80.5° in the minimized equilibrium structure was modified to 175.0°, and the EPR parameters of this new conformer were calculated without reoptimization of the structure (the new structure lies 7.85 kcal/mol above the equilibrium structure). A comparison of the spin density distributions of the two conformers (Figure S1, Supporting Information) indicates more spin density on the OH oxygen for the complex with the altered (nonequilibrium) OH orientation. The new *g* and HFC tensors reveal a considerable influence of the OH orientation. At the BPW91-40HF level, one obtains *g* values of 1.9856 (−16 685 ppm), 1.9421 (−60 236 ppm), and 1.9175 (−84 806 ppm), an isotropic HFC constant A_{iso} of 99.8 MHz, and dipolar HFC constants T_{ii} of 64.5, −33.4, and −31.1 MHz. Thus, A_{iso} is increased somewhat, the T_{ii} are slightly decreased, and all *g* values are smaller than that for the equilibrium structure. This leads to improved agreement with experiment for Δg_{11} and Δg_{22} (although Δg_{22} is now too negative) but to a much larger deviation from experiment for Δg_{33} (the component of the *g* tensor pointing toward the OH ligand), which is dramatically too negative in the new structure. The relative tensor orientation is also considerably different in the new structure. Now, the $g_{11}-A_{11}$ and $g_{33}-A_{33}$ angles (34.1° and 35.6°) are larger than those found experimentally, and the deviation from collinearity of g_{22} and A_{22} ($g_{22}-A_{22}$ angle of 20.9°) is also still larger than that for the equilibrium structure. This altered orientation together with the low g_{33} value renders the overall agreement with experiment worse. However, these results clearly indicate that the EPR parameters are sensitive to the reorientation. Such structural changes may well play a role for differences between experiment and theory in cases with conformational freedom in the direct ligand sphere of the molybdenum center. Indeed, distributions in the conformation of equatorial ligands have been discussed for sulfite oxidase sites.[72]

MoOClL[1]. This complex is similar to the first group of systems above, except that the chloro ligand does not possess any conformational degrees of freedom. For this complex, very recent single-crystal measurements determined the orientation of the *g* tensor in the molecular frame, and quantum-chemical calculations of the EPR parameters were performed, employing semiemperical INDO/S-CIS and DFT methods.[21] It seems that the experimental determination of the HFC tensor and HFC tensor orientation was difficult in the single-crystal experiment, due to disorder and convolution of two independent molecules in the unit cell.[21] The HFC tensors reported in Table 2 should thus be taken with care.

Our calculations exhibit the typical dependence on HF exchange admixture (Tables 1 and 2). Δg_{22} and Δg_{33} are already slightly too negative for more than 20% exact exchange, whereas the Δg_{11} shift is still somewhat too positive at 40% (probably due to the neglect of higher-order SO corrections[23]). Keeping the uncertainties in the experimental *A* tensor in mind, agreement with experiment may be considered as excellent at the BPW91-40HF level, in particular after the inclusion of SO corrections (Table 2). Table 3 reveals that the smallest angle between *g*- and HFC-tensor axes is found for g_{11} and A_{11} (5.9°). The $g_{22}-A_{22}$ and $g_{33}-A_{33}$ angles are 19.8°. These values are slightly increased (by 1.2°) or decreased (by 7.5°) upon the inclusion of SO corrections (cf. Table 3). As indicated above, no reliable experimental information on the orientation of the HFC tensor is available, albeit the g_{11} and A_{11} components had been assumed to be nearly covariant based on the spectral characteristics.[21]

Since single-crystal EPR measurements were done for this compound,[21] we may compare the computed and experimental *g*-tensor orientations with respect to the molecular

(72) Enemark, J. H.; Astashkin, A. V.; Raitsimring, A. M. *Dalton Trans.* **2006**, 3501.

frame. The angles between the Mo−O bond and the *g*-tensor components are computed (BPW91-40HF) to be 10°, 93°, and 99° for g_{11}, g_{22}, and g_{33}, respectively. This is in good agreement with the experimental values[21] of 10°, 94°, and 82° (some of the experimental angles were recalculated for a right-handed coordinate system; also cf. Figure 2 for an illustration). The angle between g_{22} and the Mo−S2 bond (cf. Cosper et al.[21] and Figure 2) is computed to be 170° compared with that of 143° from experiment. The single-crystal EPR analysis finally determines an angle of 38° between g_{33} and Mo−Cl whereas the calculations predict this angle to be only 7°. Considering the experimental uncertainties[21] of 5−10°, this represents a rather reasonable agreement between theory and experiment for the *g*-tensor orientation in the molecular frame (Figure S3 in the Supporting Information provides a visualization of the computed absolute *g*-tensor orientation).

Our BP86 results for *g* and HFC tensors (Tables 1 and 2) agree reasonably well with the corresponding BP86 results from Cosper et al.,[21] given the different basis sets used (and the fact that the calculations in ref 21 were based on a ZORA scalar relativistic Hamiltonian combined with Breit−Pauli SO operators). While the increased *g* anisotropy with increased HF exchange admixture may be considered moderate (Table 1), it is clear that in particular the FC contribution to A_{iso} is substantially improved at about 30−40% HF exchange admixture (Table 2). Our absolute *g*-tensor orientations and those from Cosper et al.[21] are comparable.

MoOLbdt and $[MoOLS_2CNEt_2]^+$. The next group consists of two Mo^V complexes with the same ligand (L = tris-(3,5-dimethylpyrazolyl)hydroborate anion) as the reference complexes $MoOLCl_2$ and $MoSLCl_2$ from paper I.[23] The two chlorine atoms are now replaced by two different chelating sulfur donor ligands (Figure 1). While bdt represents a dithiolene ligand (as does molybdopterin), the $S_2CNEt_2^+$ ligand renders $[MoOLS_2CNEt_2]^+$ cationic. The small positive Δg_{11} of MoOLbdt and the negative Δg_{11} for $[MoOLS_2CNEt_2]^+$ (Table 1) are well-reproduced by the calculations (even if the deviations for MoOLbdt may seem large relative to the very small experimental value of 1681 ppm). In contrast to most of the species in this study, we find BPW91-40HF to overshoot the negative Δg_{22} and Δg_{33} components for these two complexes. The best agreement for $[MoOLS_2CNEt_2]^+$ is obtained at the BPW91-30HF level, whereas even lower HF exchange admixture (B3PW91 or even BP86) would suffice for MoOLbdt. Given that we have not included higher-order SO effects,[23] the agreement for Δg_{11} is actually too good at 30−40% HF exchange. Two-component *g*-tensor calculations for this system are outside the scope of the present study, and it thus remains to be seen whether these findings are due to the specific effects of higher-order SO contributions.

For the isotropic and dipolar HFC constants, the usual increase of the absolute values with increased HF exchange admixture is observed (see above), and the SO corrections are also in the expected range (Table 2). However, for both complexes there appears to be a problem with the experimental HFC tensors. Compared with the previous systems (see above), the T_{ii} components seem to be exchanged for MoOLbdt, with the largest component (now T_{22}) being negative and the two smaller components (T_{11} and T_{33}) being positive. Importantly, the reported simulations of the experimental EPR spectra predict the *g* and HFC tensors to be coaxial whereas the calculations exhibit an angle of roughly 52° (BPW91-40HF) between g_{11} and A_{11} as well as between g_{33} and A_{33} (Table 3). In the case of $[MoOLS_2CNEt_2]^+$, the experimental analysis yields a tensor orientation ($g_{11}-A_{11}$ and $g_{33}-A_{33}$ angles of 36°) in accordance with the calculated orientation. However, here the HFC tensor is simulated to be rhombic and the calculations predict an HFC tensor of roughly axial symmetry as also found for all other related complexes. In view of the close structural similarity with $MoOLCl_2$, for which our calculations in paper I compared excellently with single-crystal data,[23] analogous *g*- and HFC-tensor orientations and symmetry might be expected. This suggests possible problems with the simulations of the experimental spectra. The EPR measurements for these two complexes were performed at X-band frequencies using frozen solutions of natural-abundance samples.[19] Thus, neither single-crystal nor multifrequency EPR studies were carried out. Most importantly, no ^{95,97}Mo-enriched samples were employed, leading to a strong (75%) overlapping signal of the $I = 0$ component, which renders a precise analysis of the HFC tensor difficult.

To unravel the discrepancies between our DFT calculations and experiment, we decided to do our own simulations of the EPR spectra. Since we do not have access to the original EPR data, we revised the simulations as follows: We started from the simulation parameters of the original reference (cf. Table 2) on one side and from parameters based on the quantum-chemical HFC tensor (BPW91-40HF data with SO corrections, cf. Table 2) on the other side. Then, we adjusted the calculated HFC parameters slightly until both simulations approached each other. The similarity of the simulated spectra then indicated that the parameter set obtained from the quantum-chemical starting parameters was at least as good as the original parameter set. This yields a new set of "experimental" HFC values to compare with. The results of this procedure are presented in more detail in Figure S9 (Supporting Information), and the new HFC values and tensor orientations are included in Tables 2 and 3, respectively. In the following, we will discuss the quantum-chemically-computed EPR parameters in the context of these new experimental values. Note that a more complete approach would be a detailed comparative spectra simulation, taking into account the fact that for such low-symmetry systems the simulations suffer from an insufficient number of data. Most likely, the original fit has not been adequate, as indicated by some minor features in the spectra. This may point to the need for the lower symmetry of the system to be taken into account.

At the BPW91-40HF level, computed values for the isotropic HFC-constant exhibit the typical moderate deviations (see above) from experiment (own simulations) for both MoOLbdt and $[MoOLS_2CNEt_2]^+$. The dipolar part (including SO corrections) is in even better agreement with experiment

(Table 2), with some overestimate of the absolute values at this level (slightly less exact exchange might thus provide even better agreement). For both complexes, the g_{22} and A_{22} axes are computed to be collinear, consistent with the revised simulations. The angle between g_{11} and A_{11} (and between g_{33} and A_{33}) is found to be about 52° for MoOLbdt and about 34° for $[MoOLS_2CNEt_2]^+$ (BPW91-40HF level), comparable to 45° and 36° in the new simulations (Table 3 and Figure S9 in the Supporting Information). As for most of the complexes, the SO−HFC corrections have only a minor influence of about 2° on the relative tensor orientation for MoOLbdt. In general, we obtain good overall agreement with experiment for these two complexes when we use our own simulation parameters. Importantly, the revised parameters and the absolute tensor orientations are also much closer to those of the structurally related $MoOLCl_2$ and $MoSLCl_2$,[23] for which reliable experimental data are available.[73] This is a significant result, as the HFC tensor of MoOLbdt has been considered unusual in comparison with related models and with molybdoenzyme active sites (see, e.g., ref 74). Apparently, this "unusual" HFC tensor was an artifact of the original[19] simulation.

$[MoOCl_2dtMe_2]^-$. This anionic complex contains also a dithiolene ligand mimicking the poor π-donor ligand[75] molybdopterin found in catalytic sites of molybdoenzymes. Agreement with the experimental g tensor is not as satisfactory as that for most of the other systems in this study: While our calculations suggest deviations from an axial tensor of only about 6 ppt, the experimental difference between Δg_{22} and Δg_{33} is 24 ppt. In particular, the Δg_{33} component is still insufficiently negative even at 60% HF exchange admixture (Δg_{11} is reproduced at 40% HF exchange, but in view of possible higher-order SO contributions,[23] this may actually already constitute too low of a value). The dependence of the HFC values on exact-exchange admixture and the size of the SO corrections to the HFC tensor (Table 2) are in the typical range (cf. above). At the BPW91-40HF level, an almost axial HFC tensor, as well as almost collinear g_{22} and A_{22} axes, and angles between g_{11} and A_{11} (and between g_{33} and A_{33}) of about 17° are found (Table 3). The influence of SO corrections on the relative tensor orientations is small.

Comparison of the HFC values and the tensor orientation with experimental data is complicated by the fact that the values from the original work,[22] obtained from simulations of EPR spectra, are very likely to be erroneous: A rhombic HFC tensor (cf. Table 2) and perfect coaxiality of the g and HFC tensor were assumed. This clearly disagrees with our calculations (indeed, at all DFT levels tested). It can be shown by simulations and is also documented in the literature, e.g., for $[MoOSL^1]^-$,[76] that parameter sets with a rhombic HFC tensor and collinear g and HFC tensors on the one hand and an axially symmetrical HFC tensor and a nonzero Euler angle β on the other hand lead to virtually indistinguishable simulated EPR spectra. This holds especially for non-enriched samples with the different molybdenum isotopes in natural abundance. Therefore, we performed similar simulations of EPR spectra as described above for several cases (the procedure is detailed in Figure S10 in the Supporting Information). The resulting revised simulation parameters are included in Tables 2 and 3. They agree well with our DFT results (particularly with BPW91-40HF including SO corrections).

$[MoO_2L^1]^-$, $[MoO_2L^2]^-$, and $[MoOSL^1]^-$. We discuss this group of three complexes last. They possess two terminal oxo and/or sulfido ligands and exhibit much larger g anisotropies than the other systems. The large g anisotropies arise from the very low g_{33} values. This holds in particular for the two dioxo complexes: $[MoO_2L^2]^-$ exhibits by far the lowest g_{33} value (1.754) of all compounds under study. The computation of these g tensors also appears somewhat more challenging than that for the other systems. Δg_{11} is, as usual, too positive, probably due to the neglect of higher-order SO contributions[23,77] (the effect appears to be somewhat more pronounced than that for the other complexes in this study; cf. Table 1). The Δg_{33} component is already too negative at the BPW91-30HF level and typically best reproduced already at the B3PW91 level. It exhibits a particularly pronounced dependence on exact-exchange admixture. Δg_{22}, finally, fits in better with the results for the other systems and is reasonably well-reproduced at the BPW91-40HF level. In any case, the differences between the three complexes (and largely also those to the other systems) are quite well-reproduced. For example, the replacement of a terminal oxo by a sulfido ligand renders Δg_{33} appreciably less negative and Δg_{11} more positive. Similarly, the effects of a replacement of two oxygen donor atoms in L^2 by sulfur in L^1 are reproduced quite well.

The larger g-tensor anisotropies for complexes with two terminal oxo ligands (and somewhat less so for systems with one oxo and one sulfido ligand) have been attributed to the presence of low-lying excited states.[16] This is true when comparing to complexes like $MoOOHL^1$. A closer analysis of the major MO contributions to the $\Delta g^{SO/OZ}$ terms (Figures S4−S8 and Table S2 in the Supporting Information) indicates, however, that the trends *within* the series have to be explained differently: The negative Δg_{33} components are dominated by SOMO-virtual couplings, with one particular excitation being dominant for the systems with two oxo and/or sulfido ligands. The analysis of matrix elements and energy denominators in the second-order perturbation expression (Table S2) shows that it is less the energy denominators and more the size of the matrix elements (both orbital Zeeman and SO matrix elements) that determine the trends in the Δg_{33} value, $[MoOSL^1]^- > [MoO_2L^1]^- > [MoO_2L^2]^-$. This indicates that the spin density is more and more of metal character and less delocalized onto the ligands along this series (as confirmed by the spin density distributions in Figure S1 and by the Mulliken spin densities in Table S3, Supporting Information). Furthermore, the character of

(73) Collison, D.; Eardley, D. R.; Mabbs, F. E.; Rigby, K.; Bruck, M. A.; Enemark, J. H. W. P. A. *J. Chem. Soc., Dalton Trans.* **1994**, 1003.
(74) Kirk, M. L.; Peariso, K. *Polyhedron* **2004**, *23*, 499.
(75) Kaupp, M. *Angew. Chem., Int. Ed.* **2004**, *43*, 546.
(76) George, G. N.; Bray, R. C. *Biochemistry* **1988**, *27*, 3603.
(77) Malkin, I.; Malkina, O. L.; Malkin, V. G.; Kaupp, M. *J. Chem. Phys.* **2005**, *123*, 244103.

Table 4. Experimental g Values for Selected Molybdoenzymes

enzyme	g_{11}	g_{22}	g_{33}
sulfite oxidase			
low pH[a]	2.007	1.974	1.968
high pH[a]	1.990	1.966	1.954
xanthine oxidase			
very rapid[a]	2.0252	1.9540	1.9411
rapid 2[a]	1.9895	1.9715	1.9640
slow[a]	1.9719	1.9671	1.9551
DMSO reductase			
wild-type 1[b]	1.9924	1.9813	1.9645
mutant (S147C)[b]	1.9981	1.9903	1.9851
formate dehydrogenase			
wild-type (Se-Cys)[c]	2.094	2.001	1.990
mutant (S-Cys)[d]	2.0180	2.0030	1.9940
polysulfide reductase			
very high g[e]	2.0165	2.0025	1.9874

[a] Reference 4. [b] George, G. N.; Hilton, J.; Temple, C.; Prince, R. C.; Rajagopalan, K. V. *J. Am. Chem. Soc.* **1999**, *121*, 1256. [c] Khangulov, S. V.; Gladyshev, V. N.; Dismukes, G. C.; Stadtman, T. C. *Biochemistry* **1998**, *37*, 3518. [d] Barber, M. J.; Siegel, L. M.; Schauer, N. L.; May, H. D.; Ferry, J. G. *J. Biol. Chem.* **1983**, *258*, 10839. [e] Reference 11.

the SOMOs in the dioxo complexes differs from those of all other systems: In complexes with only one strong π-donor oxo and/or sulfido ligand X, the SOMO is essentially orthogonal to the Mo−X vector. This holds even for $[MoOSL^1]^-$, where the SOMO is essentially orthogonal to the Mo−oxo bond and exhibits appreciable Mo−S π-antibonding character (Figure S2, Supporting Information). On the other hand, the presence of two strong π-donor oxo ligands requires the SOMO to lie in the bisector plane of the O−Mo−O angle (Figure S2). The very large g anisotropy distinguishes these complexes from the much smaller values not only of the other models but also of any EPR-spectroscopically observed Mo^V state of xanthine oxidase, of sulfite oxidase, or in fact of any Mo^V state of an enzyme active site (Table 4). The main difference with respect to the enzymatic systems is the very low g_{33} value of the model compounds. This is significant for the question of structure and bonding in molybdoenzyme Mo^V states (see below).

The Δg_{11} component obtains positive contributions from couplings between Mo-ligand bonding MOs and the SOMO (Table S2 and Figures S4−S8, Supporting Information). These are largest for $[MoOSL^1]^-$, due to the larger covalency of Mo═S compared with that of Mo═O (and the consequently higher energies of the corresponding bonding MOs). This agrees with previous notions about the role of metal−ligand covalency and "charge-transfer excitations" for the Δg_{11} component[37,69,70] (sulfur SO contributions are also nonnegligible for $[MoOSL^1]^-$; cf. Table S1 in the Supporting Information). We note in passing that earlier semiempirical INDO-based studies of bonding and g tensors in these systems[16] suffered from problems of the INDO-SCF wavefunctions in describing the systems adequately.

The dependence of the HFC tensors on HF exchange admixture follows the usual trend[23] of increased absolute values with increased admixture (Table 2), with reasonable agreement at the BPW91-40HF level, after inclusion of SO corrections. These results compare well with those obtained for the $MoOLCl_2$ complex[23] and with those for the other complexes in the present study, albeit deviations appear to be a bit larger here for the T_{ii} components. The SO corrections to the isotropic HFC constants are somewhat larger than those for the other systems. Notably, corrections to the dipolar part are drastically larger (up to 59%; cf. Table 2). This may be explained as analogous to the case of the large g anisotropies (see above): MO analyses (Table S4 in the Supporting Information) reveal that the large SO contributions to the HFC tensors are due to small energy denominators of some low-lying SOMO-virtual excitations which make up for the difference with respect to the other model complexes (e.g., $MoOClL^1$ and $MoOOHL^1$). The differences within the group of MoO_2/MoOS compounds, however, can be ascribed mainly to differences in the matrix elements (Table S4, Supporting Information; see also above).

The different nature of the SOMO for the two dioxo complexes compared to all other systems in this study is reflected also in a different g-tensor orientation (Table 3; see also Figure S3 in the Supporting Information). The g_{11} component bisects the O═Mo═O angle, g_{33} is also in the O═Mo═O plane, and g_{22} is perpendicular to it. The g and HFC tensors are computed (BPW91-40HF) to be nearly coaxial, in good agreement (deviation of about 3°) with the experimental data for $[MoO_2L^1]^-$ (none are available for $[MoO_2L^2]^-$). The SO−HFC correction does not significantly alter the relative tensor orientation for $[MoO_2L^1]^-$.

For $[MoOSL^1]^-$, the situation is completely different. The g_{11}, g_{22}, and g_{33} axes point roughly along the Mo═O, the Mo−SR, and the Mo═S bonds, respectively (Figure S3, Supporting Information). The simulation of the EPR spectra yielded an angle $\beta = 36°$ between g_{11} and A_{11} and between g_{33} and A_{33}, whereas g_{22} and A_{22} were found to be covariant.[17] Without SO corrections, BPW91-40HF calculations give a relative tensor orientation where none of the axes are collinear. In this case, the SO corrections change the HFC-tensor orientation dramatically. The angle between g_{22} and A_{22} is decreased from 37.8° to 6.8°, and the $g_{11}-A_{11}$ and $g_{33}-A_{33}$ angles are now almost equal at ca. 44.6°. The new tensor orientation is much closer to the experimental result. The striking importance of the SO−HFC correction for the HFC-tensor orientation again reflects the presence of low-lying excited states (see above). In case of the dioxo complexes, which also exhibit these low-lying states, the higher local symmetry probably prohibits a similar sensitivity.

Interestingly, all three compounds of this subgroup exhibit a dependency of the Δg_{11} shift on the choice of the functional that is opposite to the trend found for all other complexes. Usually, the calculated g shift approaches the experimental value when going from BP86 to hybrid functionals and increasing the HF exchange admixture successively. At a certain point, the values may start to deteriorate again when the effects of exact exchange are overestimated (cf. $[MoOLS_2CNEt_2]^+$ and $[MoOCl_2dtMe_2]^-$). However, for the anionic complexes considered here, the Δg_{11} shifts are already too positive at the BP86 GGA level and become even slightly more positive upon increasing exact-exchange admixture (in contrast to all other systems studied here and in paper I[23]). An MO-excitation analysis of this trend is prohibited by the

coupling terms involved with hybrid functionals. Atomic *g*-tensor analyses and Mulliken spin densities (Tables S1 and S3 in the Supporting Information) suggest that these relatively subtle, inverted trends arise from a combination of more spin density on the terminal oxo/sulfido ligands (with a particularly notable effect on g_{11} for $[MoOSL^1]^-$) and changes in the Mo SO contributions.

Implications for Molybdoenzymes and for Further Computational Studies. The major goal of this study has been to establish reliable computational methodology for the prediction and interpretation of EPR parameters for Mo^V complexes of relevance in bioinorganic chemistry. Applications of the validated DFT machinery to molybdoenzymes and their models are currently being carried out in our laboratories. Nevertheless, even the present computational results shed some new light on (a) previous experimental and computational studies of model complexes and (b) relations between the model complexes and the actual enzyme active sites.

On the side of the model complexes, it is particularly illuminating that we had to revise several of the original simulations of experimental data for low-symmetry Mo^V complexes and thus arrived at substantially different HFC tensors and tensor orientations. This demonstrates the difficulties of frozen-solution X-band studies with natural-abundance samples. It is also likely that in many other cases quantum-chemical studies may provide the necessary information to arrive at an unambiguous assignment of the experimental spectrum for low-symmetry systems, even if the calculations may still exhibit systematic quantitative deviations from experiment. A point in case is our revised "experimental" HFC tensor for MoOLbdt, which differs appreciably from the original simulation (see above and Tables 2 and 3) and thus rectifies an apparently abnormal[74] tensor and tensor orientation. In view of the very good agreement of the tensors and tensor orientations with that of single-crystal data, where available (see above and also paper I[23]), we feel confident that accurate DFT calculations will play an important role as a routine tool in this context. Notably, the present results suggest that comparative spectrum simulations with the aid of quantum-chemically computed Mo hyperfine tensors may be developed into an important instrument in the determination of the full set of EPR parameters. At the very least, the quantum-chemical parameters may serve as the starting point for the simulation.

A second observation for model complexes that may also bear on the structural interpretation of EPR spectra for molybdoenzymes is the extremely negative Δg_{33} components for the dioxo complexes and, somewhat less pronounced, for the oxo/sulfido system. No Mo^V EPR spectrum of a molybdoenzyme has ever been reported with *g* tensors anywhere near the characteristics of these three complexes (Table 4). The parameters for $[MoOSL^1]^-$ are particularly relevant in this context, as similar coordination arrangements have been discussed to give rise to the "very rapid" signal of xanthine oxidase.[4,78,79] The strongest evidence for a MoOS(dithiolene) arrangement came from ^{33}S as well as ^{17}O superhyperfine couplings.[17,78,80] However, the present calculations suggest that the large *g* anisotropy is an inherent property of the oxo/sulfido moiety, and it is not found for any of the XO signals. It remains to be seen how *g*-tensor and hyperfine data may be reconciled for the very rapid signal.

4. Conclusions

Together with the preceding paper,[23] this study suggests that unrestricted DFT calculations with hybrid functionals of around 30−40% exact-exchange admixture, a specifically designed 12s6p5d basis set for molybdenum, and IGLO-II basis sets for ligand atoms provide an excellent compromise between computational effort and accuracy to study the EPR parameters of large Mo^V complexes. There are various possible modifications of the proposed scheme, e.g., the use of smaller basis sets at more remote ligand atoms to reduce timings or the use of larger or even uncontracted metal basis sets for improved accuracy, etc., that one may consider. Nevertheless, the overall scheme appears to be robust. The inclusion of spin−orbit corrections to the molybdenum HFC constants is very important for accurate calculations, and the qualitative influence of higher-order spin−orbit effects on the *g* tensor (especially on g_{11}) should always be kept in mind when discussing *g* shifts (since an explicit computation in a two-component framework will be too expensive in many cases). While the current work has not modeled environmental effects, this is of course also possible, e.g., based on the the inclusion of explicit models for the surroundings, of dielectric continuum models, pseudopotentials, point charges, or sophisticated QM/MM approaches (see a recent review related to EPR parameter calculations of organic radicals[81]).

The deviations of the computed *g* and molybdenum HFC tensors from experiment appear to be rather systematic in most cases, provided the experimental data were reliable. For example, at the BPW91-40HF level, after the inclusion of spin−orbit corrections, isotropic HFC constants are underestimated by roughly 5%, and anisotropic HFC constants are under- or overestimated by roughly 4−16%. Importantly, we could demonstrate that the DFT calculations may also provide relative (and absolute) tensor orientations in good agreement with experiment, properties that are not experimentally straightforward to obtain (in fact, they are as yet unavailable for molybdoenzymes[21]).

In this work, we could only briefly touch on the dependence of the EPR parameters on structural and conformational effects. However, it is clear that both *g* tensors and metal HFC tensors (and their orientations) are quite sensitive to even relatively small structural changes, as demonstrated by the appreciable dependence of the EPR parameters of $MoOOHL^1$ on the orientation of the equatorial hydroxy group

(78) Greenwood, R. J.; Wilson, G. L.; Pilbrow, J. R.; Wedd, A. G. *J. Am. Chem. Soc.* **1993**, *115*, 5385.
(79) Doonan, C. J.; Stockert, A.; Hille, R.; George, G. N. *J. Am. Chem. Soc.* **2005**, *127*, 4518.
(80) Wedd, A. G.; Spence, J. T. *Pure Appl. Chem.* **1990**, *62*, 1055.
(81) Improta, R.; Barone, V. *Chem. Rev.* **2004**, *104*, 1231.

(see above). An exhaustive conformational study of this and other cases is beyond the scope of the present validation work. However, it is clear that such investigations will play an important role in unraveling similar effects, both in model complexes and in enzyme active sites, where, e.g., the conformation of SR or SH groups in the equatorial ligand plane is of substantial interest.[82,83]

Similarly, such calculations allow one, of course, to systematically study the influence of the number and type of molybdenum ligand atoms (oxygen or sulfur) or the effect of ligand protonation. Additional EPR parameters like molybdenum quadrupole coupling tensors or ligand HFC tensors should also be taken into account to be able to fully interpret experimental EPR spectra.[42] Analyses of these parameters for the Mo^V complexes of this work and paper I[23] are currently in progress.

Given the mostly systematic nature of the errors in the calculations, we feel that applications to structure elucidation of Mo^V sites are also feasible. Due to various reasons (self-interaction, nondynamical correlation effects, potential spin contamination, particularly pronounced spin polarization mechanisms), the accuracy of DFT methods for transition-metal systems is currently appreciably lower than that for organic radicals[15,81,84,85] and may not allow a distinction of very tiny conformational changes. But in many cases, not even the number or nature of molybdenum ligands in various intermediate states of the catalytic cycle of molybdoenzymes is known.[1−4,11] Here, computational approaches based on DFT are able to provide the important link between structural parameters and spin Hamiltonian parameters from simulations of EPR spectra. Hence, in the future, the DFT methods used and validated in this work can and will be applied to systems of biological relevance where experimental data is available but the structure of the molybdenum binding site is not yet resolved. One such example would be the Mo^V state of polysulfide reductase.[11] Many other examples can be found where the structures of paramagnetic intermediates in the catalytic cycle of molybdoenzymes are not entirely known but where extensive and sophisticated spectroscopical studies have been carried out.[1−4]

Acknowledgment. J.F. and P.H. acknowledge financial support by the DFG (SFB 472 "Molecular Bioenergetics"). Work in Bratislava has also been supported by the Slovak Grant Agencies APVT (No. APVV-0625-062) and VEGA (No. 2/6182/26). M.K. acknowledges financial support from the DFG (projects KA1187/4-2 and KA1187/5-2) and the Graduate College ("Modern methods of magnetic resonance") at the Universität Stuttgart and technical support from Dr. R. Reviakine. We thank Prof. T. F. Prisner and the Frankfurt Center for Scientific Computing for their support.

Supporting Information Available: Spin density distribution and SOMO plots for some of the complexes (Figures S1 and S2); figure showing *g*-tensor orientations in the molecular frame for selected Mo^V model complexes (Figure S3) as well as MO schemes and detailed analyses of the *g* shifts in terms of MO contributions for selected complexes (Figures S4−S8); simulations of EPR spectra for MoOLbdt, $[MoOLS_2CNEt_2]^+$, and $[MoOCl_2dtMe_2]^-$ (Figures S9 and S10); analyses of atomic SO and MO contributions to the *g* tensors for some of the complexes (Tables S1 and S2); Mulliken spin densities for some of the complexes (Table S3) and analysis of MO contributions to the SO−HFC corrections (Table S4); table of Cartesian coordinates of all optimized structures of the Mo^V model compounds including *g*- and HFC-tensor principal axis systems (Table S5). This material is available free of charge via the Internet at http://pubs.acs.org.

IC070341E

(82) McNaughton, R. L.; Tipton, A. A.; Rubie, N. D.; Conry, R. R.; Kirk, M. L. *Inorg. Chem.* **2000**, *39*, 5697.
(83) Davie, S. R.; Rubie, N. D.; Hammes, B. S.; Carrano, C. J.; Kirk, M. L.; Basu, P. *Inorg. Chem.* **2001**, *40*, 2632.
(84) Fritscher, J. *Phys. Chem. Chem. Phys.* **2004**, *6*, 4950.
(85) Kaupp, M. Ab initio and density functional calculations of electronic g-tensors for organic radicals. In *EPR of Free Radicals in Solids—Trends in Methods and Applications*; Lund, A., Shiotani, M., Eds.; Kluwer: Dordrecht, The Netherlands, 2003; Vol. 10, p 267.